

NO-A103 570

EQUILIBRIUM AND WAVE PROPERTIES OF TWO-DIMENSIONAL ION  
PLASMAS(U) CALIFORNIA UNIV LOS ANGELES CENTER FOR  
PLASMA PHYSICS AND FUS. S A PRASAD ET AL. JUN 87

1/1

UNCLASSIFIED

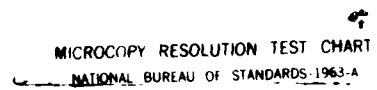
PPG-1077 N00014-75-C-0476

F/G 20/13

NL



END  
9-87  
DTIC



AD-A183 570

U E  
a

DTIC FILE COPY

"Equilibrium and Wave Properties of  
Two-Dimensional Ion Plasmas"

S.A. Prasad and G.J. Morales

June 1987

PPG-1077

DISTRIBUTION STATEMENT A

Approved for public release  
Distribution Unlimited

CENTER FOR  
PLASMA PHYSICS  
AND  
FUSION ENGINEERING  
UNIVERSITY OF CALIFORNIA  
LOS ANGELES

DTIC  
ELECTE

AUG 1 2 1987

α D

27 7 6 013

3

Contract N00014-75-C-0476

"Equilibrium and Wave Properties of  
Two-Dimensional Ion Plasmas"

S.A. Prasad and G.J. Morales

June 1987

PFG-1077

DTIC  
ELECTE  
S AUG 1 2 1987 D  
D

Department of Physics

University of California, Los Angeles

Los Angeles, CA 90024

DISTRIBUTION STATEMENT A

Approved for public release  
Distribution Unlimited

# EQUILIBRIUM AND WAVE PROPERTIES OF TWO-DIMENSIONAL ION PLASMAS

S. A. Prasad and G. J. Morales

Department of Physics  
University of California, Los Angeles  
Los Angeles, CA 90024

Accession For	
NTIS CRA&I	<input checked="" type="checkbox"/>
DTIC TAB	<input type="checkbox"/>
Unannounced	<input type="checkbox"/>
Justification	
By <i>per fti</i>	
Distribution	
Availability Codes	
Dist	Special
A-1	



Recent experiments have demonstrated the existence of collective modes in a two-dimensional single component ion layer residing just below the surface of liquid helium. A theory of the equilibrium and the wave properties of such a system is presented. The equilibrium is calculated by balancing the repulsive self-electric field pressure with the confining external electric field. In the limit of temperature  $T = 0$ , the plasma is in the form of a constant density disk at the edge of which the density decreases to zero with a scale length set by the dimensions of the enclosing cylindrical box; increasing  $T$  increases the width of the transition region. Modelling the ions as a cold two-dimensional fluid, it is found that the plasma supports an infinite set of radial modes for each value of  $l$ , the azimuthal mode number. Imposition of a constant magnetic field perpendicular to the charge sheet increases the frequency of the  $l = 0$  modes and for  $l \neq 0$ , splits each mode into two; the lowest of these split modes is related to the diocotron mode.

(1)

## I. INTRODUCTION

Recent experiments<sup>1</sup> have succeeded in confining helium ions under the surface of liquid helium. The ions form a nearly ideal two-dimensional charge disk held in position by static electric potentials applied to the walls of the confining pillbox-shaped cell and by electric fields due to the polarization of liquid helium (see Section II). Waves can be excited in the static ion system by applying an oscillating potential to a wall of the cell and sharp resonances at discrete values of the frequency have been observed.

A theory of the equilibrium and the linear wave properties of the ion system is presented here. The theory is based on the model of a classical two-dimensional fluid plasma. The equilibrium is calculated by balancing the repulsive self-electric field and the plasma pressure by the confining external electric field. In the limit of zero temperature it is found that the self-consistent plasma density is almost constant, out to some radius where the density falls to zero on a scale set primarily by the height of the confining cell. When the temperature is not zero, a Debye sheath is added to the transition region, making it wider for increasing values of the temperature. For typical experimental parameters, the ratio of the effective Debye length to the height of the cell is  $\lesssim 3 \times 10^{-4}$  and hence the zero temperature density profile is an excellent approximation to the actual profile.

To investigate the small amplitude electrostatic plasma oscillations of the ion disk, the equilibrium density profile in the zero temperature limit is used in the linearized fluid equations (governing the two-dimensional motion of the ion plasma) and in Poisson's equation (which relates the three-dimensional potential to the ion charge density). Normal modes of the system are determined by imposing the condition that the wave potential vanishes on

the conducting wall of the confining cell. It is found that an infinite set of radial modes is associated with each azimuthal mode number  $l$ . The experimentally observed resonances<sup>2</sup> can be identified with the theoretical modes corresponding to low values of the radial and azimuthal mode numbers.

An interesting consequence of the polarizability of liquid helium shows up in the plasma wave properties. One may at first sight expect that the plasma particle mass (which enters into the determination of the resonant frequencies) is  $\sim 4$  a.u. corresponding to an  $\text{He}^+$  ion. However, the force of attraction between an  $\text{He}^+$  ion and the surrounding polarized atoms of the liquid is estimated to provide enough pressure to solidify around each ion a casing of  $\sim 20$  atoms which moves together with the ion. Furthermore, since this large particle moves in a fluid, its effective mass is further enhanced<sup>3</sup> by half the mass of the displaced fluid. Thus, the effective mass is expected to be  $\sim 120$  a.u.. The value 116 a. u. gives the best agreement between theory and experiment<sup>2</sup>. This large value of the effective mass has the practical advantage of lowering the values of the resonance frequencies from those of equivalent electron systems<sup>4</sup>. The concomitant increase in the particle size ( $\sim 12 \text{ \AA}$ ) does not however cause a large viscous broadening of the plasma resonance peaks since liquid helium below 1K is almost perfectly superfluid. The observed width of the resonance peaks is believed to arise from interactions of the plasma waves with capillary waves on the liquid surface. At typical experimental temperatures of  $\lesssim 30 \text{ mK}$ , even these interactions are small and one can easily obtain sharp peaks with  $Q \sim 10^2 - 10^3$ .

Experiments have also been done<sup>5</sup> to study the effect of a constant magnetic field  $B_0 \hat{z}$  perpendicular to the plane of the ions on the wave properties of the system. The cold fluid theory is extended here to describe the

effect of the magnetic field by including the Lorentz force term in the equation of motion for a fluid element. It is interesting to note that in the presence of the magnetic field, the plasma equilibrium can be either static or dynamic. For example, in the unmagnetized cold plasma equilibrium described earlier, each fluid element is at rest since the total electric field acting on it is zero. Hence, imposing a magnetic field  $B_0 \hat{z}$  does not change the equilibrium density profile. On the other hand, one can also have dynamical equilibria with a magnetic field. For instance, if in the static magnetized equilibrium, the guard ring potential is changed, then each fluid element would experience a radial electric field. The plasma which would have adjusted its radius in the absence of  $B_0 \hat{z}$  to cancel this electric field now executes an  $\underline{E} \times \underline{B}$  rotation around the axis of the cell. Since the radial electric field is not proportional to the distance from the axis, the  $\underline{E} \times \underline{B}$  rotation velocity has a shear. Viscosity effects, if included, can also cause a radial redistribution of the plasma leading to a more complicated equilibrium problem. The present study is limited to the simple case of static equilibria.

The presence of the magnetic field breaks the azimuthal symmetry of the unmagnetized modes, i.e., modes with azimuthal mode numbers  $+l$  and  $-l$  ( $l \neq 0$ ) which are degenerate in the absence of the magnetic field now have different frequencies. These are the two-dimensional analogs of modes found in magnetized single-component plasma columns.<sup>6</sup> As in the three-dimensional case, the lowest branch (for each value of  $l$ ) is an edge mode, whose existence depends on the presence of a free plasma edge. In the limit of a large magnetic field, the density perturbation associated with this mode is localized at the plasma edge. The fluid motion is just the  $\underline{E} \times \underline{B}$  motion and

so the mode can be regarded as a two-dimensional analog of the diocotron mode.

The paper is organized as follows. In Sec. II, the geometry of a typical experiment is described and it is shown that the two-dimensional approximation of the ion system is justified. In Sec. III, the horizontal equilibrium of the charge disk is obtained by balancing the self-repulsion and pressure by the confining electric fields produced by the voltages on the cell walls. The theory points to an almost rectangular density profile with a Debye sheath near the edge. The cold fluid equations are used in Sec. IV to obtain the unmagnetized normal modes supported by a plasma disk with a rectangular radial density profile. These equations are extended to treat the magnetized modes in Sec. V.

## II. Experimental Geometry

A typical cell used in the two-dimensional ion plasma experiments is shown schematically in Fig. 1. It consists of two horizontal electrodes A and B a distance  $h$  apart, electrically insulated from a guard ring G of radius  $R$ . The cell is partially immersed in liquid  $^4\text{He}$  (a screen grid at the center of B allowing the liquid into the cell) so that the height  $d$  of liquid helium is roughly half the cell height. Helium ions are created by a field emission tip (positioned just below the screen grid in B) which is biased a large positive voltage relative to B. Once the ions enter the cell through the screen grid, they are pushed up towards the surface by the electric field due to the potential difference  $V_{AB}$  between A and B. However, the ions also polarize the surrounding liquid helium (dielectric constant  $\epsilon = 1.06$ ) and this polarization pushes the ions downwards with a force which can be simulated by image charges  $(\epsilon - 1)q/(\epsilon + 1) \approx 0.03q$  located as far above the liquid surface as the ions lie below. The two forces create a potential well for the vertical motion of the ions. The bottom of the potential well is typically  $\sim 4 \times 10^{-6}$  cm below the liquid surface (and about 20% further down at the plasma edge where the imposed vertical electric field is weaker). At typical temperatures  $\sim 3 \times 10^{-2}$  K, the r.m.s. deviation of ions about the bottom of the well is less than  $2 \times 10^{-7}$  cm. A positive potential  $V_G$  applied to the guard ring G provides the radial confinement of the plasma sheet which, typically, has a radius  $\sim 1.4$  cm and contains  $\sim 6 \times 10^8$  ions (corresponding to an interparticle spacing of  $1 \times 10^{-4}$  cm). Thus the disk formed by the ions is two-dimensional to an excellent approximation.

### III. Equilibrium

The azimuthally symmetric horizontal equilibrium of the two-dimensional plasma layer is assumed to result from the balance of the electrostatic forces on the plasma and pressure. Ignoring correlation effects, the equilibrium charge density  $\sigma_0(r)$  thus depends on the electrostatic potential  $\phi_0$  in the plane of the charges through the Boltzmann factor  $\exp(-q\phi_0/T)$  where  $q$  is the charge of a single ion and  $T$  is the temperature of the plasma (which is taken to be the temperature of the surrounding liquid helium). The equilibrium in the vertical direction  $z$  is not explicitly considered since, as indicated in the previous section, the plasma layer is a flat disk of virtually zero thickness located close to the liquid surface for typical experimental parameters. Thus, Poisson's equation can be written, to a good approximation, in the form

$$\frac{1}{r} \frac{\partial}{\partial r} r \frac{\partial}{\partial r} \phi_0 + \frac{\partial^2 \phi_0}{\partial z^2} = -4\pi q \sigma_0(r) \delta(z - d)$$

$$= -4\pi q \sigma_0(0) \exp \left\{ -q[\phi_0(r, z=d) - \phi_0(r=0, z=d)]/T \right\} \delta(z - d), \quad (1)$$

where  $\phi_0$  satisfies the boundary conditions  $\phi_0(r = R, z) = 0$ ,  $\phi_0(r, z = 0) = V_{AB} - V_G$  and  $\phi_0(r, z = h) = -V_G$  (where the zero of the potential has been redefined for convenience). It is easy to verify that

$$\phi_0(r, z) = \sum_{n=1}^{\infty} [F_n f_{0n}(z) + g_n(z)] J_0(k_{0n}r), \quad (2)$$

where

$$f_{0n}(z) = \frac{1}{\sinh k_{0n}d \sinh k_{0n}(h-d)} \begin{cases} \sinh k_{0n}d \sinh k_{0n}(h-z), & \text{for } z > d \\ \sinh k_{0n}z \sinh k_{0n}(h-d), & \text{for } z < d \end{cases} \quad (3)$$

and

$$g_n(z) = - \frac{2 \sinh k_{0n}(z-d)}{k_{0n} R J_1(k_{0n} R)} \begin{cases} V_G / \sinh k_{0n}(h-d), & \text{for } z > d \\ (V_{AB} - V_G) / \sinh k_{0n} d, & \text{for } z < d \end{cases}, \quad (4)$$

[with  $k_{0n}$  being the solutions of  $J_0(k_{0n} R) = 0$ ] is the general solution of Eq. (1) for  $z \neq d$ , which satisfies the boundary conditions and is continuous across the layer  $z = d$ .

Integration of Eq. (1) across  $z = d$  gives the jump condition

$$\frac{\partial \phi_0}{\partial z} \Big|_{d+} - \frac{\partial \phi_0}{\partial z} \Big|_{d-} = -4\pi q \sigma_0(r), \quad (5)$$

which together with Eqs. (2) - (4) yields the following nonlinear equation for the coefficients  $F_n$ :

$$\begin{aligned} & \frac{R^2}{2} J_1^2(k_{0n} R) \left\{ F_n \left[ \frac{k_{0n} \sinh k_{0n} h}{\sinh k_{0n} d \sinh k_{0n}(h-d)} \right] \right. \\ & + \frac{2}{R J_1(k_{0n} R)} \left[ \frac{V_G}{\sinh k_{0n}(h-d)} - \frac{V_{AB} - V_G}{\sinh k_{0n} d} \right] \Big\} = 4\pi q \int_0^R r dr J_0(k_{0n} r) \sigma_0(r) \\ & = 4\pi q \int_0^R r dr J_0(k_{0n} r) \sigma_0(0) \exp \left\{ -\frac{q}{T} \left[ \sum_m F_m J_0(k_{0m} r) - \sum_m F_m \right] \right\}. \end{aligned} \quad (6)$$

Equation (6) can be numerically solved for  $F_n$  and hence for  $\sigma_0(r)$  by successive iteration.

The numerical solutions indicate that as the temperature is decreased, the density profile  $\sigma_0(r)$  is almost constant up to a radius (which is determined by the geometry, the potentials applied, and the total charge) where it decreases to zero rapidly. For  $d \approx \frac{1}{2} h \ll R$ , the scale length for the density fall-off region in the small  $T$  limit is determined entirely by  $h$ , the height of the cell. Analytic solutions obtained in the Appendix

for a simple Cartesian geometry (in the  $T \rightarrow 0$  limit) supports these conclusions. The analytic solutions also suggest that the  $T = 0$  density profile near the plasma edge  $r = a$  has the form  $\sigma_0(r \approx a) \sim (a - r)^{1/2}$ . For non-zero temperatures, a Debye sheath [with Debye length defined as  $\lambda_D = (Th/4\pi q^2 \sigma_0(0))^{1/2}$ ] is added on to the plasma edge. Figure 2 displays the numerically determined equilibrium profiles  $\sigma_0(r)$  for  $\lambda_D/h = 0.1, 0.2$  and for typical experimental values  $V_G/\sigma_0(0)qh = 11.6$ ,  $V_{AB}/\sigma_0(0)qh = 9.9$ ,  $d/h = 0.467$  and  $R/h = 5$ ; these profiles are obtained by solving Eq.(6) on a radial grid of 101 points with a basis set of 82 Bessel functions. The inner profile, for which  $\lambda_D/h = 0.1$ , is a good approximation to the  $T = 0$  density profile. Typical experimental values of  $\lambda_D/h$  are less than  $3 \times 10^{-4}$  and therefore the plasma is described well by the  $T = 0$  density profile.

In the  $T = 0$  limit, there is a one-to-one correspondence between the values of the central density  $\sigma_0(0)$  and the plasma radius  $a$ , for a given geometry and a given set of confinement potentials. This relation can be obtained to a good approximation by noting that the  $T = 0$  profile is nearly rectangular and that there is no potential variation in the charge layer for  $r < a$  (i.e., no horizontal electric field for  $r < a$ ). For a rectangular profile of radius  $a$ , one can readily find the value of  $\sigma_0(0)$  needed to produce a potential drop (due to self-electric field) between  $r = 0$  and  $r = a$  which cancels the potential drop due to the external confinement fields. The result is a nearly exponential dependence of  $\sigma_0(0)$  on  $a/R$  as displayed in Fig. 3 for the values  $V_{AB} = 0.86 V_G$ ,  $d/R = 0.093$  and  $h/R = 0.2$ . The slope of the  $\ln \sigma_0(0)$  vs  $a/R$  plot is approximately  $\pi R/h$ . The maximum experimental value of  $\ln[\sigma_0(0)qh/V_G]$  that can be obtained experimentally<sup>2</sup> is  $-2.45$  corresponding to the maximum possible value of the plasma radius  $a = 0.895R = 1.34$  cm. The presence of a surface tension meniscus at the edge of the liquid

helium pool is believed responsible for limiting the plasma disk radius to this value.

As mentioned in the Introduction, the static equilibrium density profile  $\sigma_0(r)$  obtained in this section is independent of whether a magnetic field is present or not. Thus, it can be used to study both unmagnetized (Sec. IV) and magnetized (Sec. V) plasma oscillations of the ion disk. Since the width of the density fall-off region is small compared to the plasma radius, the equilibrium density profile can be approximated well by a rectangular profile. This simplifying assumption is used in the following sections.

## V. WAVES IN THE ABSENCE OF A MAGNETIC FIELD

### A. Theory

Since the equilibrium is stationary in time and is azimuthally symmetric, the perturbed density, velocity, and potential can be assumed to be proportional to  $\exp(-i\omega t + i\ell\theta)$  and thus the linearized continuity equation, equation of motion and Poisson's equation take the form

$$-i\omega\sigma_1 + \frac{1}{r} \frac{\partial}{\partial r} [r\sigma_0 v_{1r}] + \sigma_0 \frac{i\ell}{r} v_{1\theta} = 0, \quad (7)$$

$$-i\omega v_{1\perp} = -\frac{q}{m} \left( \hat{r} \frac{\partial}{\partial r} + \hat{\theta} \frac{i\ell}{r} \right) [\phi_1 + \phi_e], \quad (8)$$

$$\left( \frac{\partial^2}{\partial z^2} + \frac{1}{r} \frac{\partial}{\partial r} r \frac{\partial}{\partial r} - \frac{\ell^2}{r^2} \right) \phi_1 = -4\pi q \sigma_1 \delta(z - d), \quad (9)$$

where  $\sigma_0$ ,  $\sigma_1$  and  $v_{1\perp} = v_{1r}\hat{r} + v_{1\theta}\hat{\theta}$  are functions of  $r$ , and  $\phi_1(r, z)$  is the mode potential and  $\phi_e(r, z) \exp(-i\omega t + i\ell\theta)$  is the potential due to the driver voltage applied to the walls. It should be noted that Eqs. (7) and (8) are two-dimensional equations defined only in the plane ( $z = d$ ) of the charge layer, while Eq. (9) is a three-dimensional equation. To complete the problem, boundary conditions on  $\phi_1$  have to be specified. These are obtained by noting that the walls of the cell are conductors and that the impedance between different sections of the wall at typical mode frequencies is small; thus  $\phi_1$  can be assumed to vanish at the boundaries  $z = 0$ ,  $z = h$ ,  $r = R$  of the cell.

For  $z \neq d$ , Eq. (9) reduces to Laplace's equation for  $\phi_1$  and the general solution satisfying the boundary conditions and being continuous at  $z = d$  is

$$\phi_1(r, z) = \sum_{n=1}^{\infty} A_n f_{\ell n}(z) J_{\ell}(k_{\ell n} r) \quad , \quad (10)$$

where  $k_{\ell n}$  are the roots of  $J_{\ell}(k_{\ell n} R) = 0$  and

$$f_{\ell n}(z) = \frac{1}{\sinh k_{\ell n} d \sinh k_{\ell n} (h - d)} \begin{cases} \sinh k_{\ell n} d \sinh k_{\ell n} (h - z), & z > d \\ \sinh k_{\ell n} z \sinh k_{\ell n} (h - d), & z < d \end{cases} \quad (11)$$

is defined such that  $f_{\ell n}(z=d) = 1$ . The functions  $\sigma_1(r)$  and  $\phi_e(r, z=d)$  are also expanded in terms of  $J_{\ell}(k_{\ell n} r)$ :

$$\sigma_1(r) = \sum_{n=1}^{\infty} B_n J_{\ell}(k_{\ell n} r) \quad , \quad (12)$$

$$\phi_e(r, z=d) = \sum_{n=1}^{\infty} C_n J_{\ell}(k_{\ell n} r) \quad . \quad (13)$$

Integrating Eq. (9) across  $z = d$  gives the jump condition

$$\left. \frac{\partial \phi_1}{\partial z} \right|_{d+} - \left. \frac{\partial \phi_1}{\partial z} \right|_{d-} = -4\pi q \sigma_1(r) \quad . \quad (14)$$

Combining Eqs. (7) - (14) yields the relation

$$A_n = - \sum_{m,p} (D_1^{-1})_{nm} (D_2)_{mp} C_p \quad (15)$$

between the Fourier-Bessel components  $A_n$  of  $\phi_1(r, z=d)$  and the components  $C_n$  of the known driver potential  $\phi_e(r, z=d)$ , with the matrices  $D_1$  and  $D_2$  defined by

$$(D_1)_{mn} = (D_2)_{mn} - \frac{\omega^2}{2\omega_p^2} \frac{R}{h} \frac{k_{\ell n}^R \sinh k_{\ell n} h}{\sinh k_{\ell n} d \sinh k_{\ell n} (h - d)} J_{\ell+1}^2(k_{\ell n} R) \delta_{mn} \quad (16)$$

and

$$(D_2)_{mn} = \int_0^R r dr \hat{\sigma}_o(r) [k_{\ell m} k_{\ell n} J_{\ell}'(k_{\ell m} r) J_{\ell}'(k_{\ell n} r) + \frac{\ell^2}{r^2} J_{\ell}(k_{\ell m} r) J_{\ell}(k_{\ell n} r)] \quad . \quad (17)$$

In these definitions,  $\delta_{mn}$  is the Kronecker delta function, primes represent derivatives with respect to the arguments, and  $\omega_p^2$ ,  $\hat{\sigma}_0$  are defined as

$$\omega_p^2 = \frac{4\pi q^2 \sigma_0(0)}{mh}, \quad (18)$$

$$\hat{\sigma}_0(r) = \frac{\sigma_0(r)}{\sigma_0(0)}. \quad (19)$$

Equations (15) and (16) imply that the plasma response has resonances at frequencies for which  $\text{Det}(D_1) = 0$ . The resonance frequencies, when normalized in terms of  $\omega_p$ , are completely specified by the values of  $h/R$ ,  $d/R$  and  $\hat{\sigma}_0(r/R)$ . The numerical solutions for the lowest few resonance frequencies when  $\hat{\sigma}_0(r)$  is assumed to be a step function of radius  $a$  are displayed in Fig. 4 for typical experimental values,  $h/R = 0.2$ ,  $d/R = 0.093$ ,  $a/R = 0.895$ . Each plasma resonance is characterized by an azimuthal mode number  $\ell$  and a radial mode number  $N$ . The (numerically smoothed) functions  $\phi_1(r, z=d)$ ,  $\sigma_1(r)$ ,  $v_{1r}(r)$  and  $v_{1\theta}(r)$  are displayed in Fig. 5 for a frequency close to the  $\ell = 1$ ,  $N = 2$  resonance chosen as a typical example. Since from Eqs. (7) and (8),  $\sigma_1$  contains a term proportional to  $\partial\sigma_0/\partial r \cdot \partial\phi_1/\partial r = -\sigma_0(0)\delta(r-a)\partial\phi_1/\partial r$  and since the radial electric field does not vanish at  $r = a$ ,  $\sigma_1$  has a sharp spike at the plasma edge. It is, however, noticed in the numerical solutions (as in Fig. 5) that  $\phi_1(r < a, z=d)$  has the form of a single Bessel function with a rather small derivative at  $r = a$  (as long as  $a/R$  is not very close to unity). In fact, the assumption  $\phi_1 = \hat{A}_N J_\ell(K'_{\ell N} r) \hat{f}_{\ell N}(z)$  [where  $K'_{\ell N}$  is a solution of  $J'_\ell(Ka) = 0$  and  $\hat{f}_{\ell N}$  is defined by Eq. (11) with  $K'_{\ell N}$  taking the place of  $k_{\ell N}$ ] can be used in Eqs. (7) - (9) to obtain good approximations to the resonance frequencies  $\omega_{\ell N}$  of a step-function equilibrium density profile:

$$\omega_{\ell N}^2 = \omega_p^2 \frac{h}{a} \frac{K'_{\ell N} a \sinh K'_{\ell N} d \sinh K'_{\ell N} (h - d)}{\sinh K'_{\ell N} h} . \quad (20)$$

Equation (20) predicts that when plotted versus  $K'_{\ell N} a$ , the resonance frequencies for all  $\ell$  fall on the same curve. The solid line in Fig. 6 represents this curve for  $d/a = 0.104$ ,  $h/a = 0.223$ . The exact numerical solutions ( $d/a = 0.106$ ,  $h/a = 0.223$ ,  $a/R = 0.895$ ) using the expansion (10) for  $\phi_1$  lie very close to this curve. The assumption  $d\phi/dr = 0$  at the conducting wall ( $r = R$ ) has been used previously <sup>1, 7</sup> to obtain an equation similar to Eq. (20) which agrees well with the experimental values of resonance frequencies. Figure 6 shows why this assumption works well (even though it is unjustified) when  $a$  is nearly equal to  $R$ . The limits of applicability of Eq.(20) are discussed later.

The simple approximate structure of  $\phi_1$  suggested by the numerical results can be understood by considering Eqs. (7) -(9), which can be combined, ignoring  $\phi_e$ , as

$$\omega^2 \nabla^2 (\phi_1 e^{i\ell\theta}) = \nabla_{\perp} \cdot \left[ \frac{4\pi q^2}{m} \sigma_o(r) \nabla_{\perp} (\phi_1 e^{i\ell\theta}) \right] \delta(z - d) . \quad (21)$$

Multiplying both sides by  $\phi_1 \exp(-i\ell\theta)$  and integrating over the cell volume yields the variational (Rayleigh-Ritz) principle value of  $\omega^2$  ,

$$\omega^2 = \omega_p^2 \frac{\int_0^a r dr \hat{\sigma}_o(r) \left| \nabla_{\perp} [\phi_1(r, z=d) e^{i\ell\theta}] \right|^2}{\int_0^R \int_0^h r dr dz \left| \nabla [\phi_1(r, z) e^{i\ell\theta}] \right|^2} . \quad (22)$$

The minimum value of the right-hand side gives the lowest eigenvalue  $\omega^2$  and the  $\phi_1$  that makes it the minimum is the corresponding eigenfunction. The second lowest eigenvalue is the minimum produced by a wave function which is orthogonal to the first and so on. It is of interest to note that Eq. (22) [along with Eq. (8)] implies that the total energy in the wave electric field is equal to the total kinetic energy of the plasma particles.

To proceed further, the denominator in Eq. (22) is converted, on integration by parts, into the area integral  $4\pi q \int_0^a r dr \sigma_1 \phi_1 (r, z = d)$ . From Eqs. (14), (11), (10), and (12), it follows that if  $k_{\ell n} h \ll 1$ , then

$$B_n \approx \frac{1}{4\pi q} \frac{h}{d(h-d)} A_n ;$$

thus if  $h/R$  is small and if higher order Fourier-Bessel components can be ignored, then

$$\sigma_1(r) \approx \frac{1}{4\pi q} \frac{h}{d(h-d)} \phi_1(r, z=d). \quad (23)$$

Thus Eq. (22) takes the form

$$\omega^2 = \omega_p^2 d(h-d) \frac{\int_0^a \left| \nabla_{\perp} [\phi_1(r, z=d) e^{i\ell\theta}] \right|^2 r dr}{\int_0^a \left| \phi_1(r, z=d) e^{i\ell\theta} \right|^2 r dr} . \quad (24)$$

The minima of the ratio of the integrals can be verified to be  $(K'_{\ell N})^2$  [which occur for  $\phi_1 = J_{\ell}(K'_{\ell N} r)$ ] in agreement with Eq. (20) in the limit of small  $h/R$ .

The discussion above suggests that Eq. (20) might fail when the value of  $h/R$  is not small compared to unity. Figure 7 displays how the deviation between the prediction of Eq. (20) [solid line] for the  $\ell = 0, N = 2$  mode chosen as an example and the exact numerical solutions of Eqs. (15) - (17) [circles] increases with increasing values of  $h/R$ . Figure 8 presents the comparison between the predictions of Eq. (20) [solid line] for the same mode and the exact numerical solutions [circles] as a function of  $a/R$  for  $h/R = 0.2$ . The percentage difference is relatively constant until  $a/R \approx 0.98$ , beyond which it rapidly increases. The limiting value of the exact solution as the plasma edge approaches the walls can be obtained from Eqs. (15) - (17). For  $a/R \rightarrow 1$ , the matrix  $D_2$  becomes diagonal,

$$(D_2)_{mn} = \frac{k_{\ell m}^2 R^2}{2} J_{\ell+1}^2(k_{\ell m} R) \delta_{mn}, \quad (25)$$

and thus the resonance frequencies (which are the zeros of  $D_1$ ) have the values

$$\omega_{\ell N}^2 = \omega_p^2 \frac{h}{R} \frac{k_{\ell N} R \sinh k_{\ell N} d \sinh k_{\ell N} (h-d)}{\sinh k_{\ell N} h}, \quad (26)$$

corresponding to wave functions  $\phi_1 = B_N J_{\ell}(k_{\ell N} r) f_{\ell N}(z)$  which vanish at  $r = R$ . It is found numerically that the transition from the modes of Eq. (20) (whose radial derivative at the plasma edge is small) to the modes of Eq. (26) (whose value at the plasma edge vanishes) occurs for values of  $a/R$  very close to unity ( $a/R > 0.98$  for typical values of  $h/R$ ). The frequencies of Eq. (26) are roughly  $(k_{\ell N}/K'_{\ell N})^2$  higher than the values of Eq. (20). Since in experiments, the plasma radius  $a$  cannot approach the cell radius  $R$  to within  $\sim 1.5$  mm due to the liquid helium meniscus, modes described by Eq. (26) cannot be observed in cells with  $R < 8$  cms.

## B. Comparison with Experiments

Waves are excited in the experiments of Ref. 1 by imposing an oscillating potential  $\phi_w$  on the guard ring and are detected by measuring the current from a circular button (of radius  $r_c$ ) at the center of the top electrode. If the apparatus is exactly cylindrically symmetric, only  $l = 0$  modes should be detected. The values predicted by Eq. (20) for the first four radial modes having no angular dependence agree with the experimental values to within a few percent. Other resonances have also been observed<sup>2</sup>, which can be identified with the predictions of Eq. (20) for various low values of  $l (\neq 0)$  and  $N$ ; these probably arise from an undetermined azimuthal asymmetry in the system.

For the  $l = 0$  modes, the absolute value of the current flowing out of the center button when the driver frequency matches a resonant frequency [given approximately by Eq. (20)], can be obtained by including the collisional damping term  $\nu_{11}$  on the left-hand side of Eq. (8). This has the effect of replacing  $\omega^2$  in Eq. (16) by  $\omega(\omega + i\nu)$ . If  $\nu$  is small compared to the frequencies  $\omega$  of interest, this is equivalent to replacing  $\omega$  by  $\omega + i\nu/2$  in Eq. (16). For  $\omega$  near  $\omega_{0N}$  [which are simple zeros of  $D_l(\omega)$  as follows from the self-adjointness of Eq. (21)], one can write

$$D_l^{-1}(\omega + i\nu/2) \approx \frac{\nu}{\omega - \omega_{0N} + i\nu/2} D_l^{-1}(\omega_{0N} + \nu),$$

where  $D_l^{-1}$  on the right hand side can be conveniently evaluated at a real value  $\omega_{0N} + \nu$  of the frequency. From Eq. (15) a similar relation holds for the coefficients  $A_n$  evaluated at  $\omega + i\nu/2$ . Therefore, from Eq. (10) the wave potential has the form

$$\phi_l(r, z) = \sum_{n=1}^{\infty} \frac{\nu A_n(\omega_{ON} + \nu)}{\omega - \omega_{ON} + i\nu/2} f_{ON}(z) J_0(k_{ON}r)$$

when  $\omega$  is close to  $\omega_{ON}$  and  $\nu$  is small compared to  $\omega$ . The real coefficients  $A_n(\omega_{ON} + \nu)$  are obtained by numerically solving Eq. (15) for  $\omega = \omega_{ON} + \nu$  and

$$C_n = -2\phi_w [\sinh k_{On} d + \sinh k_{On} (h-d)] [k_{On} R J_1(k_{On} R) \sinh k_{On} h]^{-1}.$$

The charge density induced on the center button by the plasma wave potential is  $q\sigma_{ind} = (4\pi)^{-1} \partial\phi_l / \partial z|_{z=h}$  and the magnitude of the current through the center button is given by

$$\begin{aligned} I(\omega = \omega_{ON}) &= \omega [2\pi \int_0^{r_c} r dr |\sigma_{ind}|] \\ &= \frac{1}{2} (\omega r_c) \left| \sum_{n=1}^{\infty} \frac{\nu A_n(\omega_{ON} + \nu)}{[(\omega - \omega_{ON})^2 + \nu^2/4]^{1/2}} \frac{J_1(k_{ON} r_c)}{\sinh k_{ON} (h-d)} \right|. \end{aligned} \quad (28)$$

For  $\omega$  not too close to  $\omega_{ON}$ , one can ignore  $i\nu/2$  and replace the terms in the braces by  $A_n(\omega)$ . The plot of  $I(\omega)$  vs.  $\omega$  consists of a series of Lorentzian resonance peaks centered at  $\omega_{ON}$  and of width  $\nu$ . This is displayed in Fig. 9 for a typical value of the collision frequency  $\nu = 4 \times 10^{-3} \omega_p$  and for a range of  $\omega$  covering the first four  $l = 0$  resonances.

V. WAVES IN THE PRESENCE OF A MAGNETIC FIELD  $\mathbf{B} = B_0 \hat{z}$

Imposing a uniform magnetic field  $\mathbf{B} = B_0 \hat{z}$  perpendicular to the plane of the plasma disk introduces the Lorentz force term  $\Omega \mathbf{v}_{1\perp} \times \hat{z}$  (where  $\Omega = qB_0/mc$  is the cyclotron frequency) to the right-hand side of the linearized equation of motion (8). Thus the perturbed velocity components are given by

$$v_{1r} = \frac{1}{\omega^2 - \Omega^2} \frac{q}{m} \left( -i\omega \frac{\partial}{\partial r} + \frac{i\ell\Omega}{r} \right) [\phi_1 + \phi_e]_{z=d}, \quad (29a)$$

$$v_{1\theta} = \frac{1}{\omega^2 - \Omega^2} \frac{q}{m} \left( \frac{\ell\omega}{r} - \Omega \frac{\partial}{\partial r} \right) [\phi_1 + \phi_e]_{z=d}. \quad (29b)$$

Using the expansions (10) - (13) for  $\phi_1$ ,  $\sigma_1$ , and  $\phi_e$ , one again obtains Eq. (15), but with the matrices  $D_1$  and  $D_2$  now given by

$$(D_1)_{mn} = (D_2)_{mn} - \frac{\omega^2 - \Omega^2}{2\omega_p^2} \frac{R}{h} \frac{k_{\ell n} R \sinh k_{\ell n} h}{\sinh k_{\ell n} d \sinh k_{\ell n} (h - d)} J_{\ell+1}^2(k_{\ell n} R) \delta_{mn}, \quad (30)$$

$$(D_2)_{mn} = \int_0^R r dr \hat{\sigma}_0(r) [k_{\ell m} k_{\ell n} J'_\ell(k_{\ell m} r) J'_\ell(k_{\ell n} r) + \frac{\ell^2}{r^2} J_\ell(k_{\ell m} r) J_\ell(k_{\ell n} r)] \\ + \frac{\ell\Omega}{\omega} \int_0^R r dr \frac{d\hat{\sigma}_0(r)}{dr} J_\ell(k_{\ell m} r) J_\ell(k_{\ell n} r). \quad (31)$$

If  $\ell = 0$  or if  $\hat{\sigma}_0$  is constant for  $0 \leq r \leq R$ , then the last term of Eq. (31) vanishes; then Eqs. (30) and (31) can be obtained from Eqs. (16) and (17) by replacing  $\omega^2$  by  $\omega^2 - \Omega^2$ . Thus, the square of the resonance frequencies in the magnetized case are shifted up by an amount  $\Omega^2$  from the unmagnetized values with the eigenfunctions remaining unchanged. These are the two-dimensional analogs of the usual upper hybrid resonance.

Without the last term in Eq. (31), modes corresponding to  $+l$  and  $-l$  are degenerate. For  $l \neq 0$  and  $d\hat{\sigma}_0/dr \neq 0$  (for some  $r < R$ ), the last term in Eq. (31) breaks the degeneracy and causes each unmagnetized mode to split into two upper hybrid modes which propagate in opposite directions with azimuthal phase velocities  $\omega/l$ . In addition, two modes appear near  $\omega = \Omega$ , corresponding to  $+l$  and  $-l$ . The effect of the magnetic field for  $|l| = 1$  is shown in Fig. 10 for  $a/R = 0.895$ ,  $d/R = 0.093$  and  $h/R = 0.2$ , where  $a$  is the width of the rectangular density profile  $\hat{\sigma}_0(r)$ . The modes occur in pairs designated  $+$  or  $-$  depending on whether they propagate circularly right handed or left handed with respect to the magnetic field. The two new modes near  $\omega = \Omega$  are also shown. It should be noted that while these modes occur very close to the cyclotron frequency  $\Omega$ , there is no resonance when  $\omega = \Omega$  exactly. It is of interest to note that when  $\omega = \Omega$  exactly, Eqs. (30) and (15) yield  $D_1 = D_2$  and  $A_n = -C_n$ . Thus the density perturbation produced in the plasma is such that the total wave potential  $\phi_i + \phi_e$  is zero in the plane of the charges. This is true for all values of  $l$  including  $l = 0$ .

The forms of  $\phi_l(r, z = d)$  and  $\sigma_l(r)$  for the magnetized modes are qualitatively similar to the corresponding magnetized modes. The wave potential  $\phi_l(r, z = d)$  for the positive  $l$  mode near  $\omega = \Omega$  increases linearly with  $r$  till the plasma edge and then decreases to zero at  $r = R$ ; the perturbed density  $\sigma_l$  increases monotonically to a peak at  $r = a$ , as displayed in Fig. 11 for the case  $l = +1$ . The curves are obtained by numerically solving Eq. (15) for  $h/R = 0.2$ ,  $d/R = 0.093$ ,  $a/R = 0.895$ ,  $\Omega/\omega_p = 0.5$  and  $\omega/\omega_p = 0.504$ . A basis set of 82 Bessel functions is used on a 101-point radial grid; the oscillations in  $\phi_l$  for  $r > a$  and the finite height of  $\sigma_l$  at  $r = a$  are consequences of these numerical limitations. For the negative  $l$  mode near  $\omega = \Omega$ ,

the wave potential  $\phi_1(r, z = d)$  is mainly confined to the annulus  $a < r < R$  and the perturbed density  $\sigma_1$  is localized at the plasma edge  $r = a$ .

The behavior of the magnetized modes is similar to the unmagnetized modes as  $a/R$  approaches unity. In this limit, the last term in Eq. (31) vanishes, the matrix  $D_2$  becomes diagonal, and the resonance frequencies take the values

$$\omega_{\ell N}^2 = \Omega^2 + \omega_p^2 \frac{h}{R} \frac{k_{\ell N} R \sinh k_{\ell N} d \sinh k_{\ell N} (h-d)}{\sinh k_{\ell N} h} \quad (32)$$

As in the unmagnetized case, the frequencies of Eq. (32) correspond to eigenmodes  $\phi_1(r, z = d) \sim J_{\ell}(k_{\ell N} r)$ . It is worth noting that without a free plasma edge, the  $+\ell$  and  $-\ell$  modes are degenerate even in the presence of a magnetic field.

As  $a/R$  increases towards 1, the frequencies of the  $\pm \ell$  modes (for any given value of  $\Omega$ ) shift to the values  $\omega_{\ell N}$  given by Eq. (32) accompanied by a corresponding change in the form of  $\phi_1(r, z = d)$ ; the exceptions are the  $-\ell$  mode near  $\omega = \Omega$  which approaches  $\omega = \Omega$ , and the lowest  $+\ell$  mode which approaches  $\omega = 0$ . As in the unmagnetized case, the change is rather abrupt near  $a/R \approx 0.99$ . As shown in Fig. 10 (for  $|\ell| = 1$ ), the bottom two  $+\ell$  modes cross each other and it becomes clear upon letting  $a/R$  approach unity that there is a mode transition at the crossing. This is illustrated in Fig. 12 for the case  $\ell = 1$ . The two upper lines go over to  $\omega_{11}$  given by Eq. (32) in the limit  $a/R \rightarrow 1$  and must be regarded as the same mode. Similarly the lower two lines approach  $\omega = 0$  in the limit  $a/R = 1$  and hence belong to the same branch. For the lowest branch, for all  $\ell \neq 0$ , the ratio  $\omega/\Omega$  approaches zero for large values of  $\Omega$  and in this limit, Eq. (29) yields  $x_{11} = -(c/B) \nabla_{\perp} (\phi_1 + \phi_e)_{z=d} \times \hat{z}$  indicating incompressible motion

( $\nabla_{\perp} \cdot \tilde{v}_{\perp} = 0$ ) along the plane of the charges. Also from the continuity equation,  $\sigma_1 = (i\omega)^{-1} v_{1r} d\sigma_0/dr = -(i\omega)^{-1} v_{1r} \sigma_0(0) \delta(r-a)$ ; thus the perturbed charge density is localized at the plasma edge  $r = a$ . The mode in the limit of large  $\Omega$  is purely an edge mode and can be interpreted as a two-dimensional analog of the usual diocotron mode. It should however be noted that the two-dimensional equilibrium considered here does not execute an  $\tilde{E} \times \tilde{B}$  rotation and hence phenomena such as negative energy waves and resonance layers are absent in the present system.

## VI. CONCLUSIONS

A theory of the equilibrium and wave properties of a two-dimensional ion plasma confined just below the surface of liquid helium has been developed. In equilibrium, it is found that for the typical confinement geometry used in experiments, the plasma density profile is almost rectangular in the cold limit; for  $T \neq 0$ , a Debye sheath is introduced at the edge. A theory of linear waves that considers the plasma as a cold two-dimensional fluid has been constructed. Imposing the condition that the linearized wave potential vanish at the conducting walls of the confining cell leads to an infinite set of radial modes for each value of the azimuthal mode number  $\ell$ . Through a variational approach, it is shown that an excellent analytical approximation for these frequencies can be obtained (for  $h/R \ll 1$  and  $a/R$  not very close to unity) and that the wave potential in the plane of the charges for any resonant frequency has the form of a Bessel function with a rather small derivative at the plasma edge. Imposition of a uniform, constant magnetic field perpendicular to the plane of the charges does not change the equilibrium of the system in the  $T = 0$  limit. However, the frequencies of the  $\ell = 0$  normal modes are shifted upwards and for  $|\ell| \neq 0$ , each normal mode is split into two modes (corresponding to  $+\ell$  and  $-\ell$ ) which propagate azimuthally in opposite directions. Two new modes ( $+\ell$  and  $-\ell$ ) appear for frequencies very close to the cyclotron frequency. The two lowest  $+\ell$  modes cross each other and it is shown that there is a mode transition at that point. The lower branch is an edge mode and is identified as the two-dimensional analog of the diocotron mode. The other branches are the analogs of the familiar upper hybrid mode.

VII. ACKNOWLEDGEMENTS

We thank Professor G. Williams, S. Hannahs and A. Greenfield for useful discussions concerning their experiments which motivated the present study.

This work was sponsored by the Office of Naval Research.

## APPENDIX

### EQUILIBRIUM PROFILE IN CARTESIAN GEOMETRY

A simplified model geometry in which the equilibrium density profile of the two-dimensional plasma can be analytically obtained in the zero temperature limit is described here. The model, shown in Fig. 13, is a Cartesian model, one in which the plasma is a ribbon infinitely long in the direction perpendicular to the plane of the figure. The notation is slightly different from that of Fig. 1. The vertical coordinate is now denoted by  $y$  (with  $z$  used to denote the complex variable  $x + iy$ ). Also, for convenience the plasma layer is assumed to be midway between the top and the bottom of the confining box. As in Sec. II, the vertical equilibrium is not explicitly considered and consequently the vertical holding field is ignored. Thus, the model consists of a ribbon of charge constrained (by forces not included in the analysis) to the midplane of the containing cell. The self-repulsion of the plasma particles balances the confining force due to the potential  $V_0$  applied to the side walls and thus determines the horizontal equilibrium density profile  $\sigma_0(x)$ . Since the temperature is assumed to be zero, the plasma pressure plays no role in the equilibrium.

Because the horizontal electric field on each plasma particle is zero,  $\phi(x, y = 0) = V_1 = \text{constant}$  for  $|x| \leq a$ . From symmetry, the lines AB and OD in Fig. 13 are lines of force. One thus has the problem of finding the charge distribution on OA when it is at potential  $V_1$ , the side BC is at 0, the side CD at  $V_0$  with AB and OD being lines of force. Conformal mapping is used to solve for the potential distribution and hence the charge density on OA. The potential  $V_1$  is not known a priori, but it is found that for only one particular value of  $V_1$  is the calculated charge density finite everywhere in OA and has the correct sign; this special value of potential must be that corresponding to the equilibrium in the cold limit.

The interior of the rectangle OBCD can be mapped into the upper half of the complex  $\zeta$ -plane by the elliptic function transformation

$$\zeta = \xi + i\eta = m \operatorname{sn}^2[K(m)(1 + \frac{iz}{d}), m] , \quad (A1)$$

where  $z = x + iy$ . Defining the parameter  $m$  by the equation

$$\frac{d}{L} = \frac{K(m)}{K'(m)} , \quad (A2)$$

it is seen that the points D, O, A, B, C in the  $z$ -plane are mapped into  $\zeta_D = 0$ ,  $\xi_O = m$ ,  $\xi_A$ ,  $\xi_B = 1$ ,  $\xi_C = \infty$  of the  $\zeta$ -plane, with the interior of the rectangle DOBC mapped into the upper half of the  $\zeta$ -plane (Fig. 14a). To keep the solution reasonably simple, it is also assumed that the plasma half-width  $a$  is such that  $\xi_A = 1 - m$ ; from Eq. (A1), this implies

$$\xi_A = m \operatorname{nd}^2[K'(m) \frac{a}{L}, 1 - m] = 1 - m. \quad (A3)$$

The problem thus reduces to finding a function  $P = \psi + i\phi$  analytic in the upper half of the  $\zeta$ -plane with  $\phi$  satisfying the conditions indicated in Fig. 14a, along the real axis. The solution to the problem is the superposition of the complex potentials satisfying the boundary conditions of Figs. 14b and 14c. The respective solutions are

$$P_b = iV_1 + \frac{\frac{1}{2} V_0 - V_1}{K'([1 - 2m]^2)} \operatorname{sn}^{-1} \left[ \frac{2\zeta - 1}{1 - 2m}, (1 - 2m)^2 \right] , \quad (A4)$$

$$P_c = -\frac{iV_0}{4} \left[ 1 + \frac{2}{\pi} \operatorname{sn}^{-1} \frac{2(2\zeta - 1)^2 - \{1 + (1 - 2m)^2\}}{1 - (1 - 2m)^2} \right] . \quad (A5)$$

The surface charge density of the plasma sheet is given by

$$\begin{aligned}
 -\frac{1}{2\pi q} \frac{d\phi}{dy} \Big|_{y=0, |x| \leq a} &= \frac{-1}{2\pi q} \operatorname{Re} \frac{dP}{dz} \Big|_{y=0, |x| \leq a} \\
 &= -\frac{K'(m)}{\pi q L} \frac{1}{(1-m-\xi)^{1/2}} \left[ \frac{\frac{1}{2} V_0 - V_1}{2K'([1-2m]^2)} - \frac{V_0}{\pi} \left( \xi - \frac{1}{2} \right) \right]. \quad (A6)
 \end{aligned}$$

The surface charge density has a singularity at  $\xi = 1 - m$  [or from Eq. (A3),  $x = a$ ] unless

$$\frac{\frac{1}{2} V_0 - V_1}{2K'([1-2m]^2)} + \frac{V_0}{2\pi} = \frac{V_0}{\pi} (1 - m)$$

or

$$V_1 = V_0 \left[ \frac{1}{2} + \frac{2m-1}{\pi} K'([1-2m]^2) \right], \quad (A7)$$

in which case the charge density is

$$\begin{aligned}
 \sigma_0(x) &= \frac{K'(m)V_0}{\pi^2 q L} \operatorname{Re}(1-m-\xi)^{1/2} \\
 &= \frac{K'(m)V_0}{\pi^2 q L} \operatorname{Re} \{ 1 - m - m \operatorname{nd}^2 [K'(m) \frac{x}{L}, 1-m] \}^{1/2}. \quad (A8)
 \end{aligned}$$

The dependence of  $\sigma_0$  on  $x$  is displayed in Fig. 15 for the value  $d/L = 0.625$  (or  $m = .1$ ). To demonstrate that the warm plasma density profile approaches this shape in the limit  $T \rightarrow 0$ , the numerical solutions of the Cartesian analog of Eqs. (1) - (6) are also shown in Fig. 15 for the same geometry, the same  $\sigma_0(0)$  and  $\lambda_D/d = 0.05$  and  $0.1$  [where  $\lambda_D = \{(2dT/4\pi q^2 \sigma_0(0))\}^{1/2}$ ].

For small values of  $m$  [or from Eq. (A2), small values of  $d/L$ ], Eq. (A8) can be expanded near  $x = a$  to find the behavior of the density profile near the edge. This yields

$$\frac{\sigma_o(x \approx a)}{\sigma_o(x = 0)} = \text{Re} \left[ \pi m^{1/2} \frac{a - x}{d} + \left( \frac{\pi}{2} \frac{a - x}{d} \right)^2 \right]^{1/2} . \quad (\text{A9})$$

Thus, very near the plasma edge  $x = a$ ,  $\sigma_o(x) \sim (a - x)^{1/2}$ . The width of the plasma edge is approximately  $2d/\pi$ .

The  $(a - x)^{1/2}$  dependence for  $\sigma_o(x \approx a)$  can also be obtained from a simpler argument. The solution of the two-dimensional Laplace's equation

$$\frac{\partial^2 \phi}{\partial x^2} + \frac{\partial^2 \phi}{\partial y^2} = 0 \quad (\text{A10})$$

in the vicinity of  $x = a$  (see Fig. 16) has the general form

$$\phi(\rho, \theta) = \text{Re} \sum_{n=0}^{\infty} P_n (\rho e^{i\theta})^{n+s} + V_1 , \quad (\text{A11})$$

where  $\rho = [(x - a)^2 + y^2]^{1/2}$  and  $\theta = \tan^{-1} [y/(x - a)]$ . Applying the conditions  $\phi(\rho, \pi) = V_1$ ,  $(1/\rho) \partial \phi / \partial \theta|_{\theta=0} = 0$  and the fact that the electric field is finite everywhere leads to the expression

$$\phi(\rho, \theta) = V_1 + \sum_{n=1}^{\infty} Q_n \rho^{n+1/2} \cos[(n + \frac{1}{2})\theta] . \quad (\text{A12})$$

The charge density for  $x < a$  is

$$\sigma_0(x < a) = \frac{1}{p} \frac{\partial \phi}{\partial \theta} \Big|_{\theta=\pi} = \frac{3}{2} Q_1 (a - x)^{1/2} - \frac{5}{2} Q_2 (a - x)^{3/2} + \dots \quad (A13)$$

in agreement with Eq. (A9).

In the cylindrical case, Laplace's equation for the equilibrium potential is (with  $z$  = vertical coordinate in the notation of Sec. III)

$$\frac{\partial^2 \phi}{\partial r^2} + \frac{1}{r} \frac{\partial \phi}{\partial r} + \frac{\partial^2 \phi}{\partial z^2} = 0 \quad (A14)$$

which can be locally (for  $r \approx a$ ) transformed into the form (A10) by setting  $r = a \exp(\epsilon u)$ ,  $z = \epsilon a v$  in the limit  $\epsilon \rightarrow 0$ . Following the same procedure, one can show that even in the cylindrical case, the equilibrium density profile  $\sigma_0(r \approx a) \propto (a - r)^{1/2}$ .

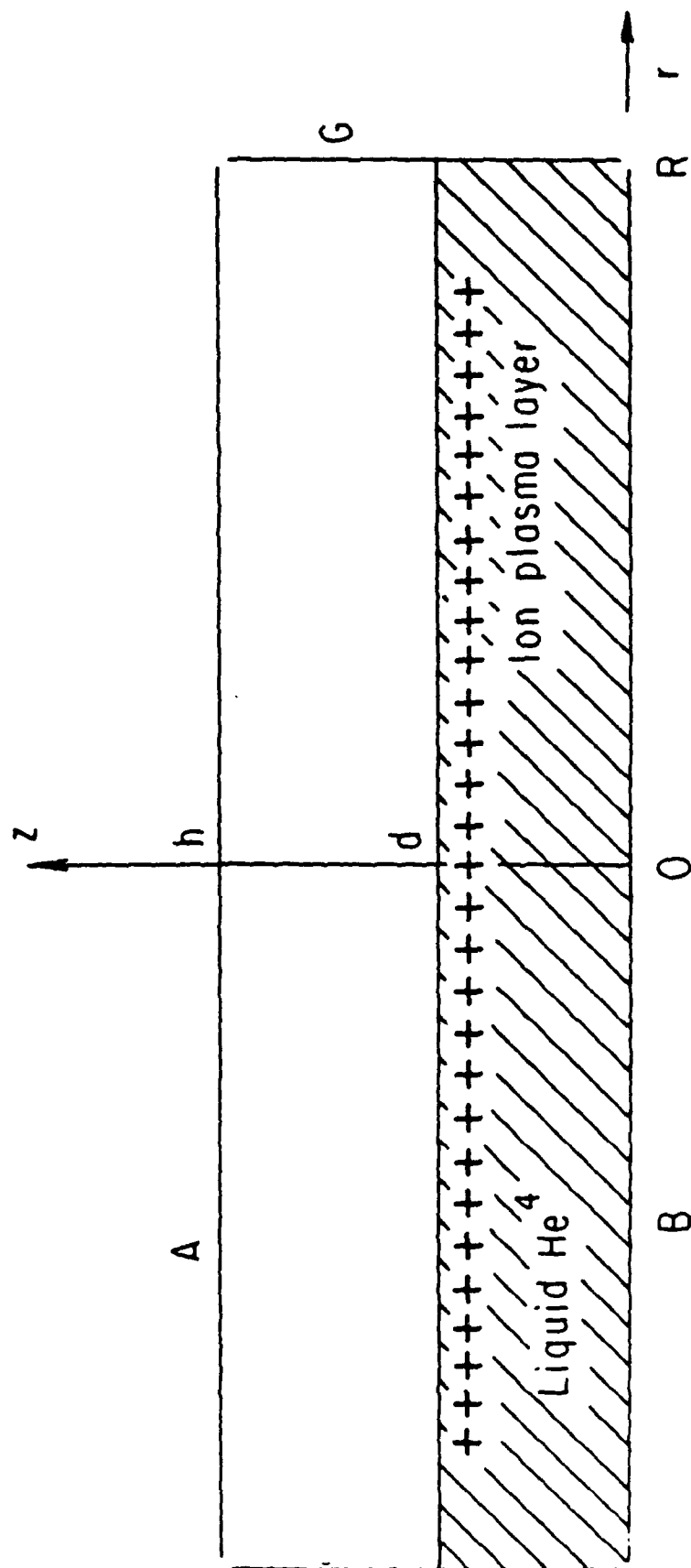
REFERENCES

1. M. L. Ott-Rowland, V. Kotsubo, J. Theobald and G. A. Williams, Phys. Rev. Lett. 49, 1708 (1982).
2. G. A. Williams (private communication).
3. L. D. Landau and E. M. Lifshitz, "Fluid Mechanics" (Pergamon, Oxford, 1959), ch. 1, sec. 11.
4. C. C. Grimes and G. Adams, Phys. Rev. Lett. 36, 145 (1976). For a recent survey of two-dimensional electron and ion layers at liquid helium surface, see Ref. 5.
5. A. J. Dahm and W.F. Vinen, Physics Today, February 1987, p43.
6. R. C. Davidson, "Theory of Nonneutral Plasmas" (Benjamin, Reading, Mass., 1974), chap. 2.
7. D. S. Fisher, B. I. Halperin and P.M. Platzman, Phys. Rev. Lett. 42, 798 (1979).

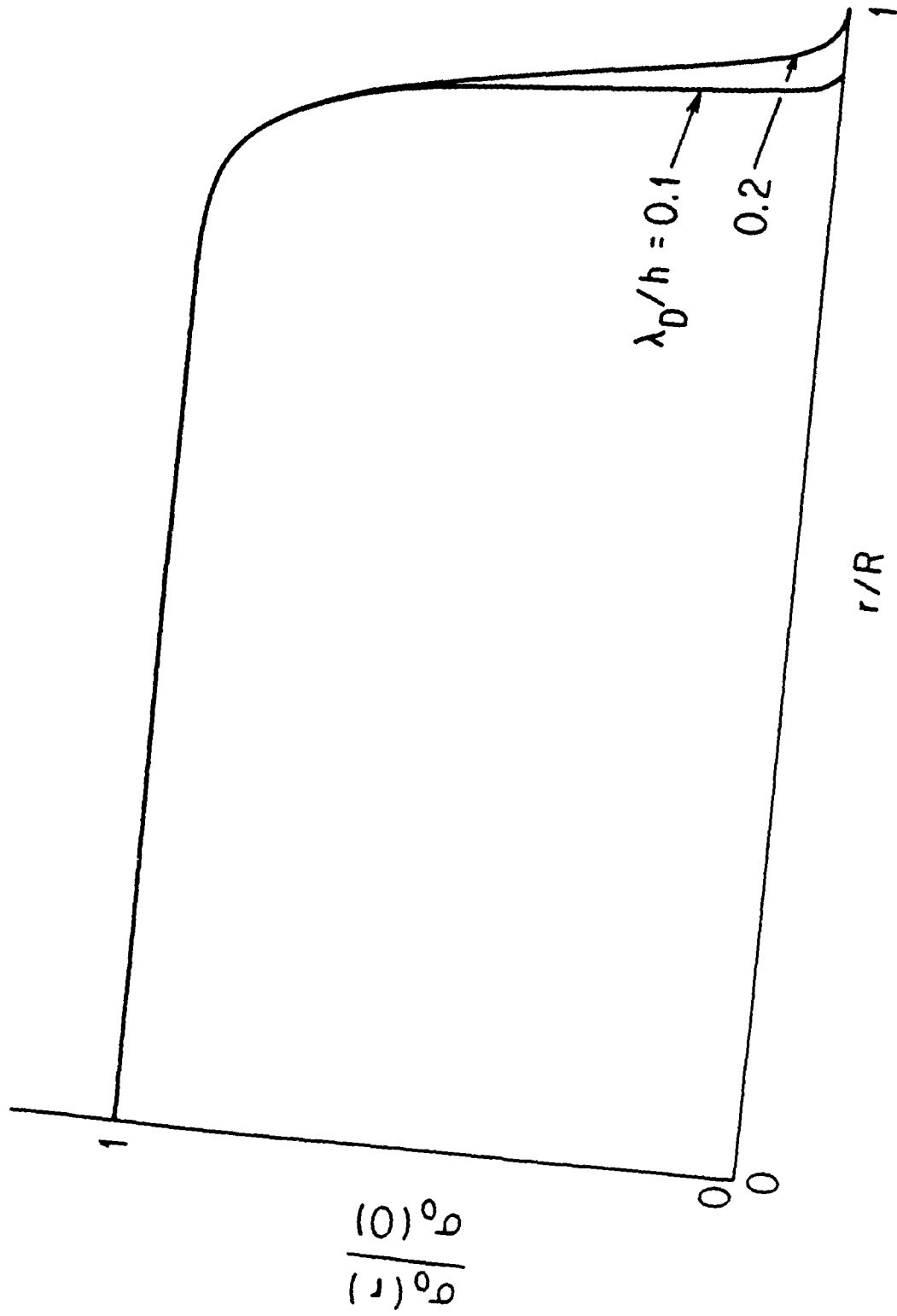
FIGURE CAPTIONS

1. Typical experimental geometry.
2. Equilibrium density profiles  $\sigma_0(r)$  for  $\lambda_D/h = 0.1, 0.2$  and for typical experimental values  $V_G/\sigma_0(0)qh = 11.6$ ,  $V_{AB}/\sigma_0(0)qh = 9.9$ ,  $d/h = 0.467$  and  $R/h = 5$ .
3. Central density  $\sigma_0(0)$  required to produce a plasma disk of radius  $a$  for  $T = 0$ ;  $V_{AB} = 0.86V_G$ ,  $d/R = 0.093$  and  $h/R = 0.2$ .
4. Unmagnetized normal mode frequencies for  $d/R = 0.093$ ,  $h/R = 0.2$  and  $a/R = 0.895$ . The modes are characterized by azimuthal mode number  $\ell$  and radial mode number  $N$ .
5. Radial dependence of wave potential  $\phi_1(r, z=d)$ , density  $\sigma_1(r)$ , radial velocity  $v_{1r}(r)$  and azimuthal velocity  $v_{1\theta}(r)$  for the  $\ell = 1$ ,  $N = 2$  mode; the geometry parameters are  $d/R = 0.093$ ,  $h/R = 0.2$  and  $a/R = 0.895$ . If  $\phi_1$  is real,  $\sigma_1$  and  $v_{1\theta}$  are also real and  $v_{1r}$  is purely imaginary [see Eqs. (7)-(9)].
6. Comparison of the exact values of the resonance frequencies and the approximate values given by the analytical expression (20) [solid line] for  $d/a = 0.104$ ,  $h/a = 0.223$  and  $a/R = 0.895$ .
7. Comparison, as a function of  $h/R$ , of exact values of resonance frequencies (circles) and the approximate values given by the analytic expression (20) [solid line] for the  $\ell = 0$ ,  $N = 2$  mode and for  $a/R = 0.895$ ,  $d/h = 0.465$ .
8. Comparison, as a function of  $a/R$ , of exact values of resonance frequencies (circles) and the values given by Eq. (20) [solid line] for the  $\ell = 0$ ,  $N = 2$  mode and for  $d/R = 0.093$ ,  $h/R = 0.2$ .

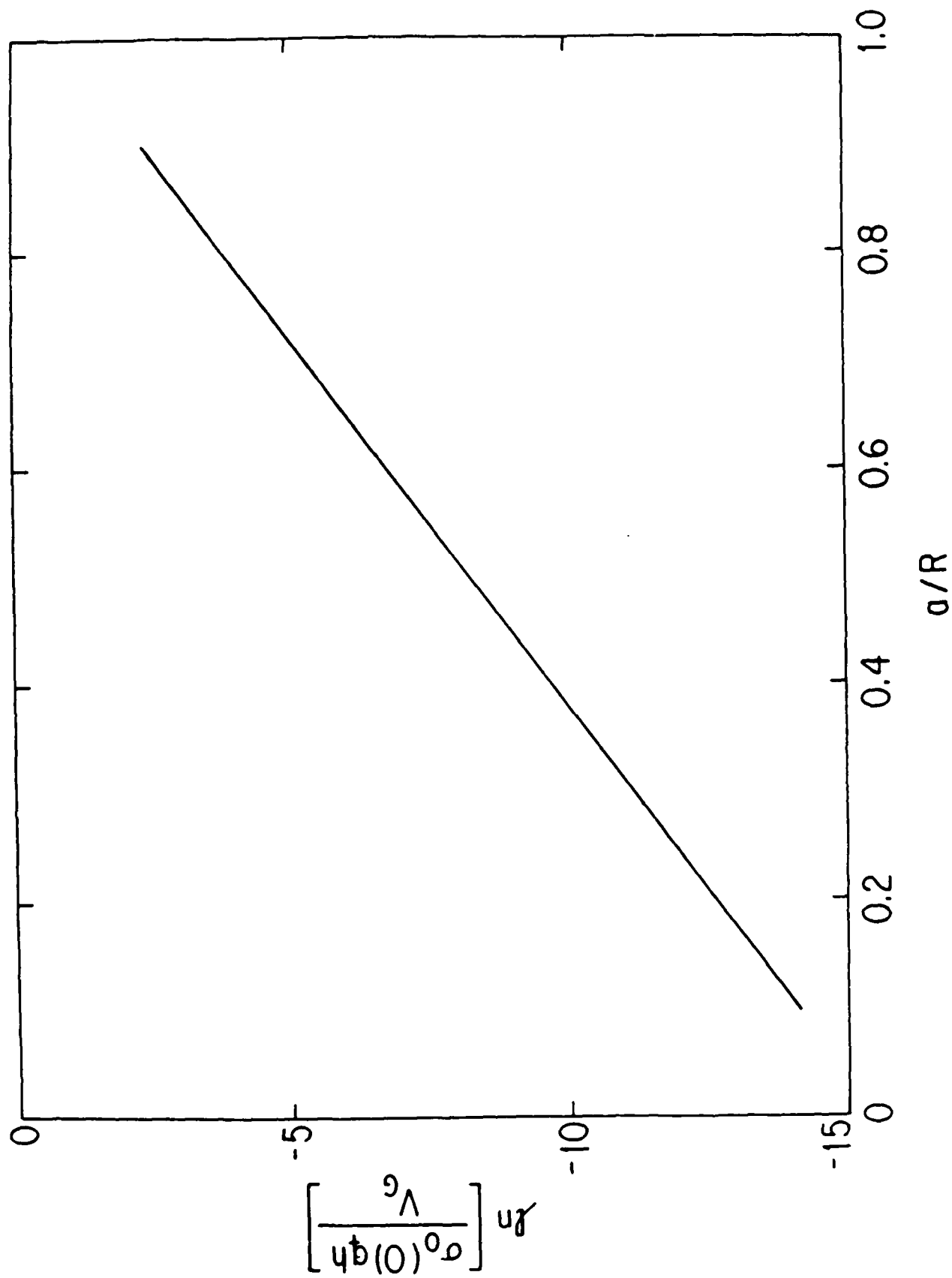
9. Current  $I$  (in amperes) through the center button in the top electrode as a function of the external frequency  $\omega$  [Eq. 28]. The collision frequency  $\nu$  is  $4 \times 10^{-3} \omega_p$  and the driver voltage  $\phi_w = 10\text{mV}$ .
10. Plasma resonances vs.  $\Omega = qB/mc$  for  $\ell = \pm 1$  and for  $d/r = 0.093$ ,  $h/R = 0.2$ ,  $a/R = 0.895$ . The branches designated + (or -) propagate circularly right-handed (or left-handed) with respect to the magnetic field.
11. Radial dependence of the potential  $\phi_1(r, z=d)$  and density  $\sigma_1(r)$  for the  $\ell = +1$  mode near  $\omega = \Omega$  for  $\Omega/\omega_p = 0.5$ ,  $d/R = 0.093$ ,  $h/R = 0.2$ ,  $a/R = 0.895$ .
12. Enlargement of the region where the  $\ell = +1$  modes cross in Fig. 10. The positions of the branches as  $a/R$  assumes the values 0.895, 0.985 and 1.0 are shown.
13. Cartesian model geometry for the confined two-dimensional plasma layer.
14. a) Complex  $\zeta$ -plane showing the mapping (A1). The shaded area (rectangle OBCD) of Fig. (13) is mapped into the upper half of the  $\zeta$ -plane. The problem can be regarded as a superposition of two potential problems illustrated in (b) and (c).
15. Density profile  $\sigma_0(x)$  given by the analytic expression (A8) for  $d/L = 0.625$  or  $m = 0.1$  (thick line). The other curves are numerical solutions of the Cartesian analogs of Eqs. (1) -(6) for the same geometry, the same  $\sigma_0(0)$  and for  $\lambda_D/d = 0.05$  and 0.1; the Debye length  $\lambda_D$  is defined as  $\lambda_D = [2dT/4\pi q^2 \sigma_0(0)]^{1/2}$ .
16. Geometry in the vicinity of the plasma edge  $x = a$ .



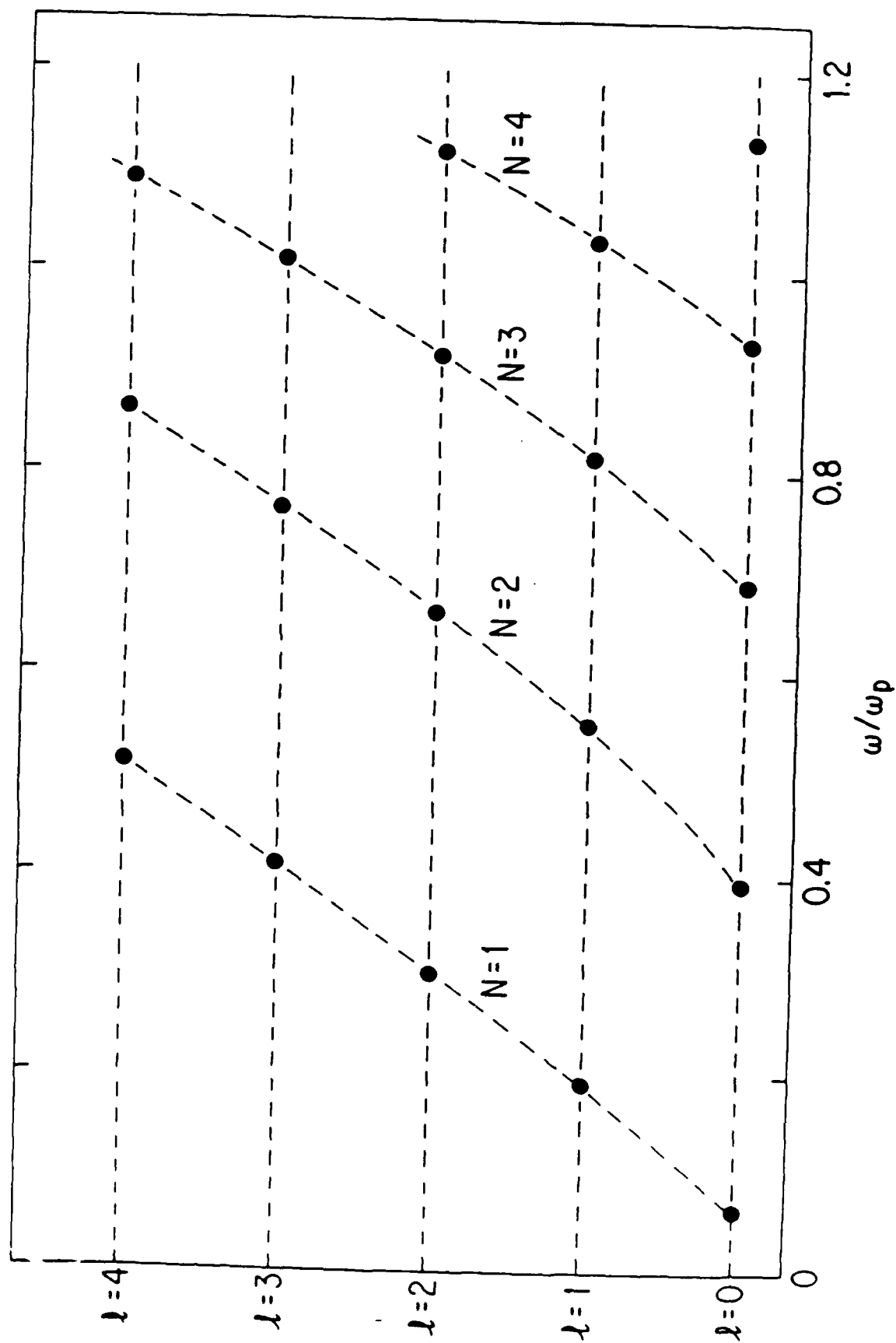
1. Typical experimental geometry.



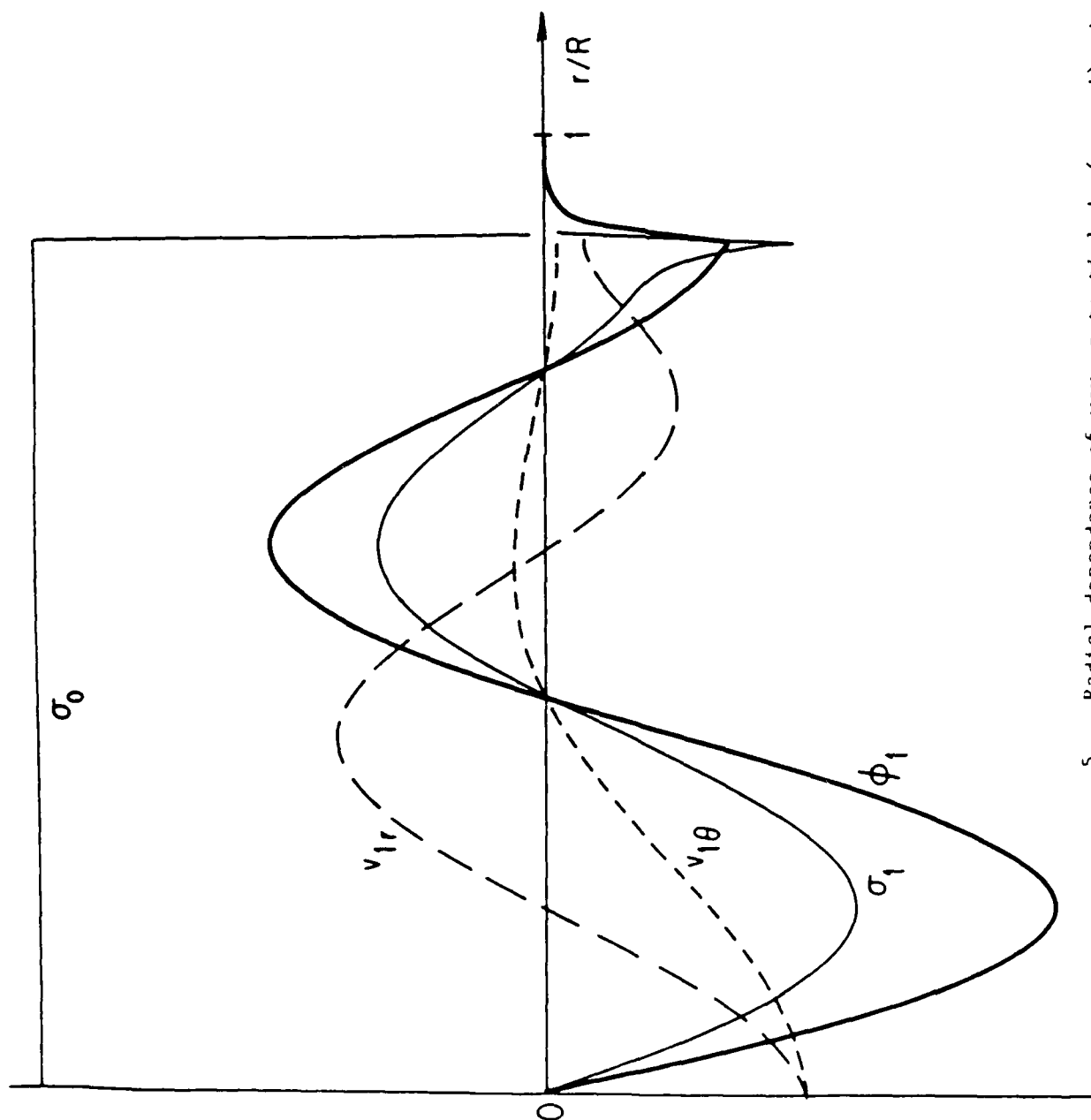
2. Equilibrium density profiles  $\sigma_0(r)$  for  $\lambda_D/h = 0.1, 0.2$  and for typical experimental values  $V_G/\sigma_0(0)qh = 11.6$ ,  $V_{AB}/\sigma_0(0)qh = 9.9$ ,  $d/h = 0.467$  and  $R/h = 5$ .



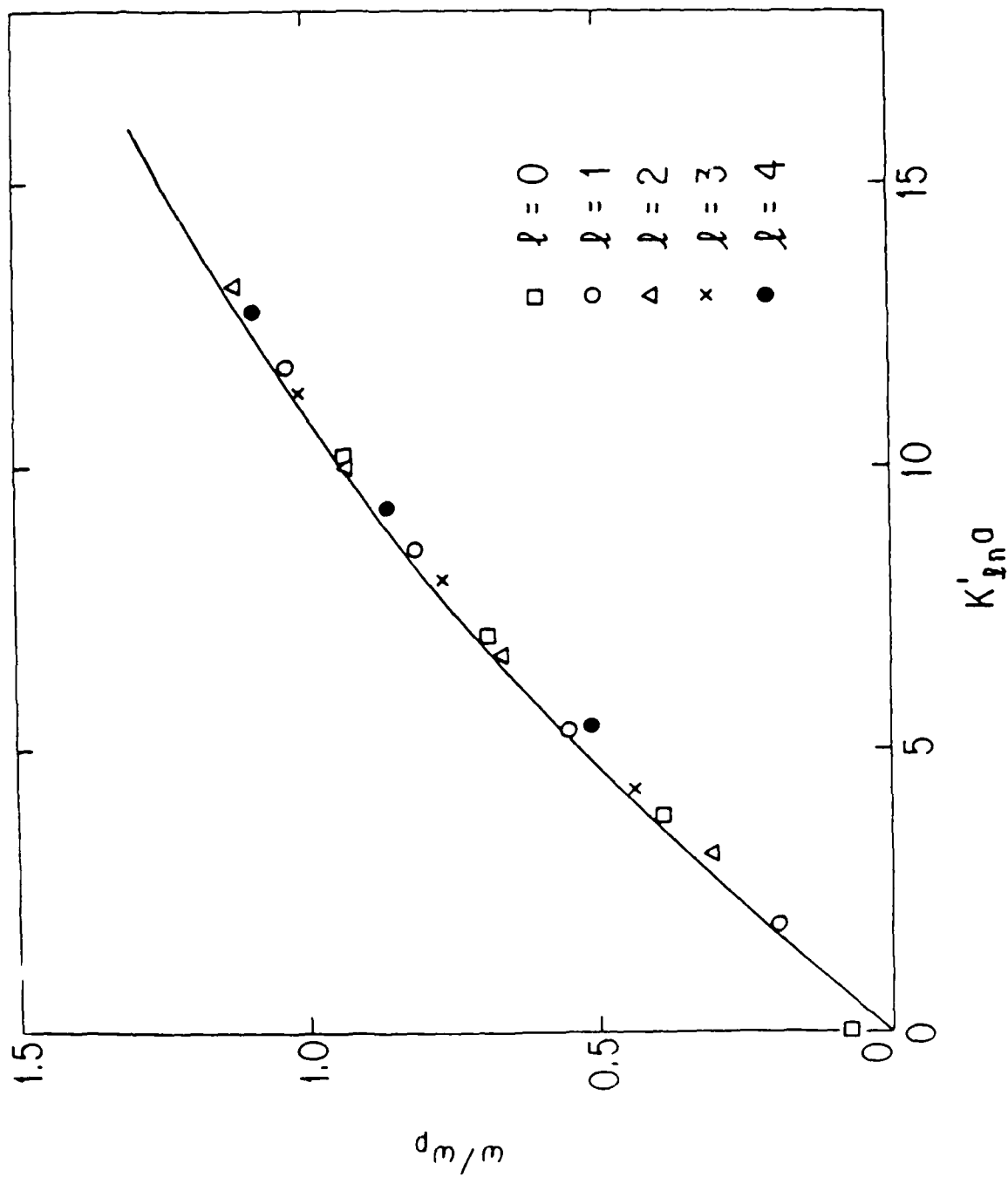
3. Central density  $\sigma_0(0)$  required to produce a plasma disk of radius  $a$  for  $T = 0$ ;  $V_{AB} = 0.86V_0$ ,  $d/R = 0.093$  and  $h/R = 0.2$ .



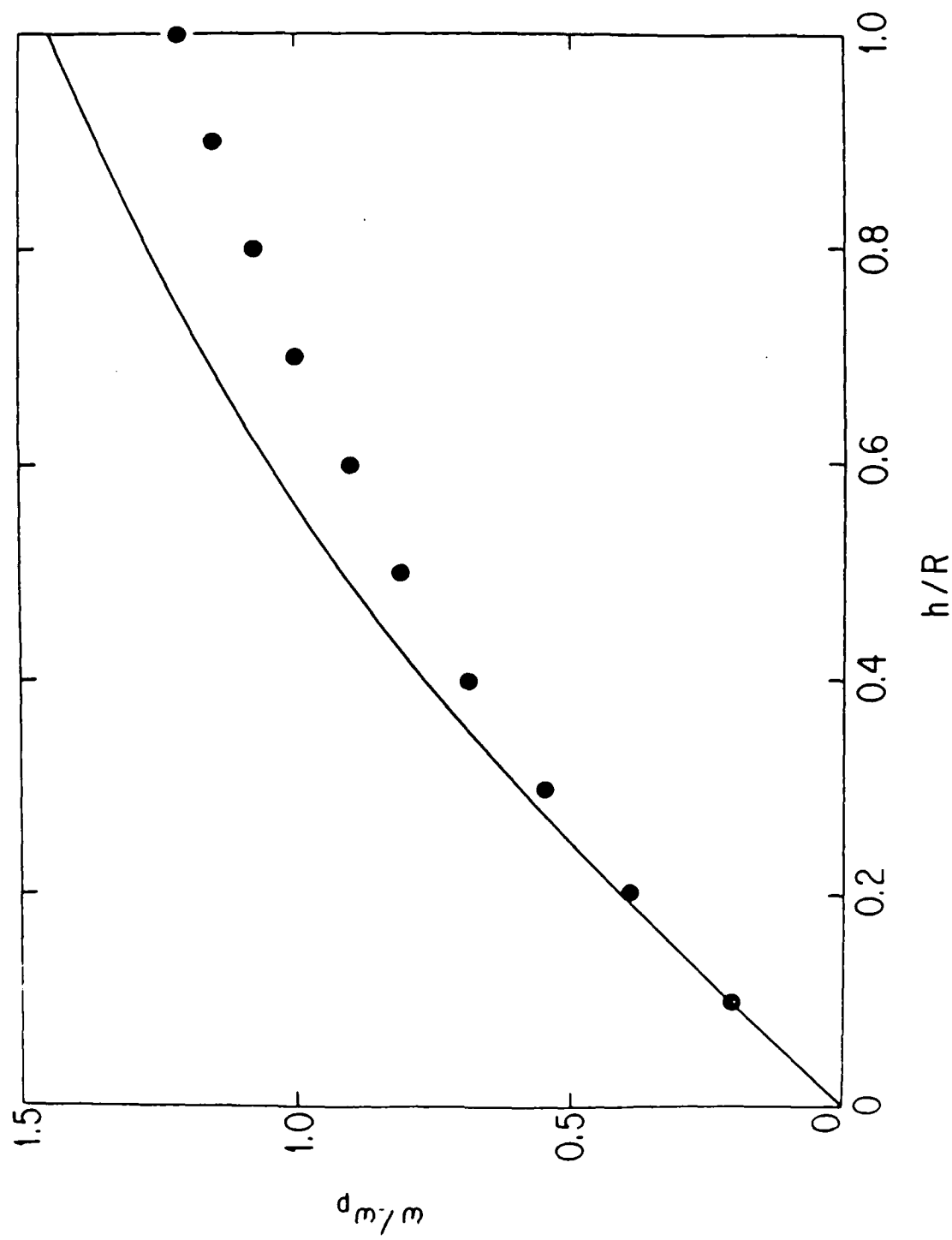
4. Unmagnetized normal mode frequencies for  $d/R = 0.093$ ,  $h/R = 0.2$  and  $a/R = 0.895$ . The modes are characterized by azimuthal mode number  $l$  and radial mode number  $N$ .



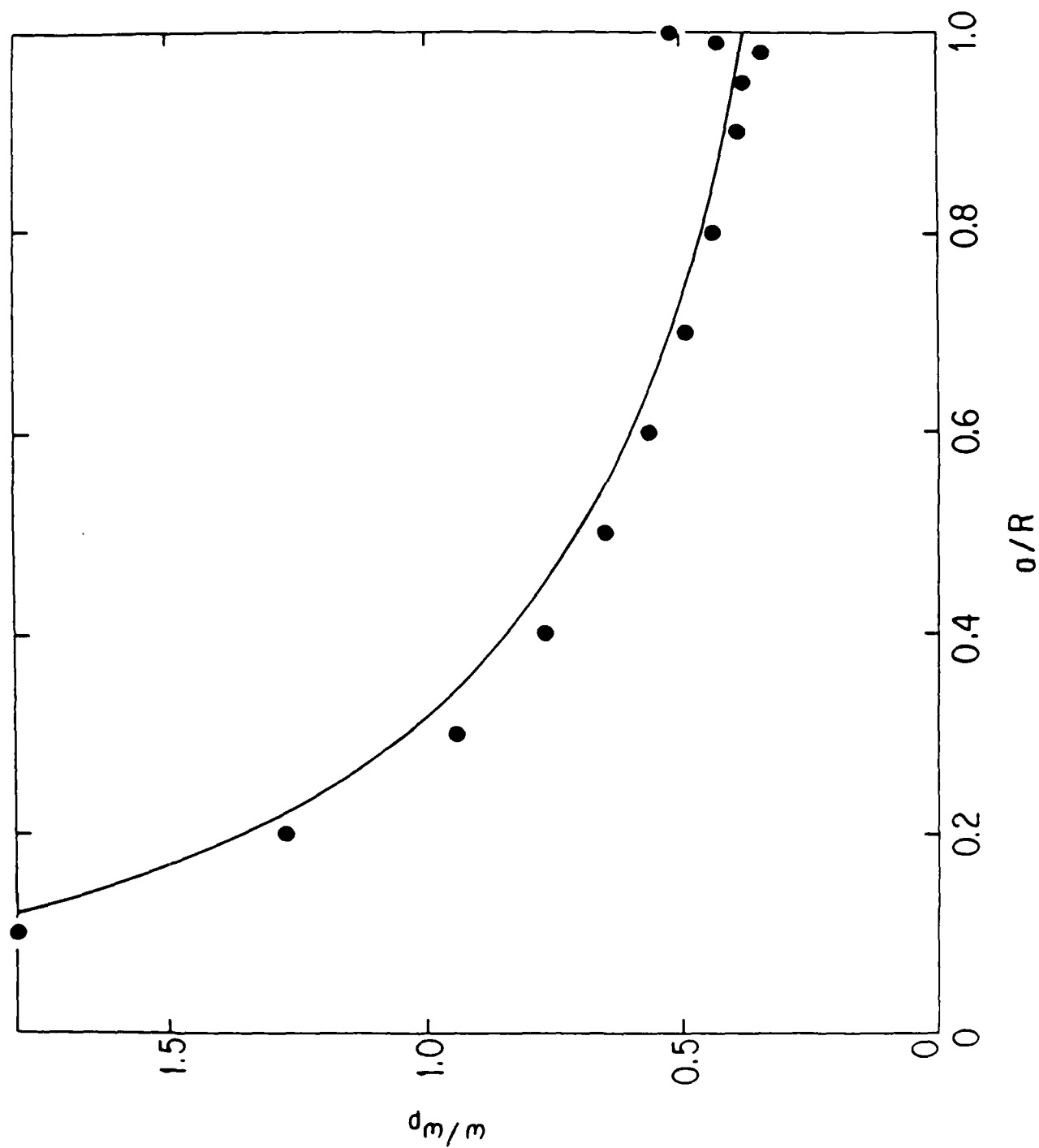
5. Radial dependence of wave potential  $\phi_1(r, z=d)$ , density  $\sigma_1(r)$ , radial velocity  $v_{1r}(r)$  and azimuthal velocity  $v_{1\theta}(r)$  for the  $l = 1$ ,  $N = 2$  mode; the geometry parameters are  $d/R = 0.093$ ,  $h/R = 0.2$  and  $a/R = 0.895$ . If  $\phi_1$  is real,  $\sigma_1$  and  $v_{1\theta}$  are also real and  $v_{1r}$  is purely imaginary [see Eqs. (7)-(9)].



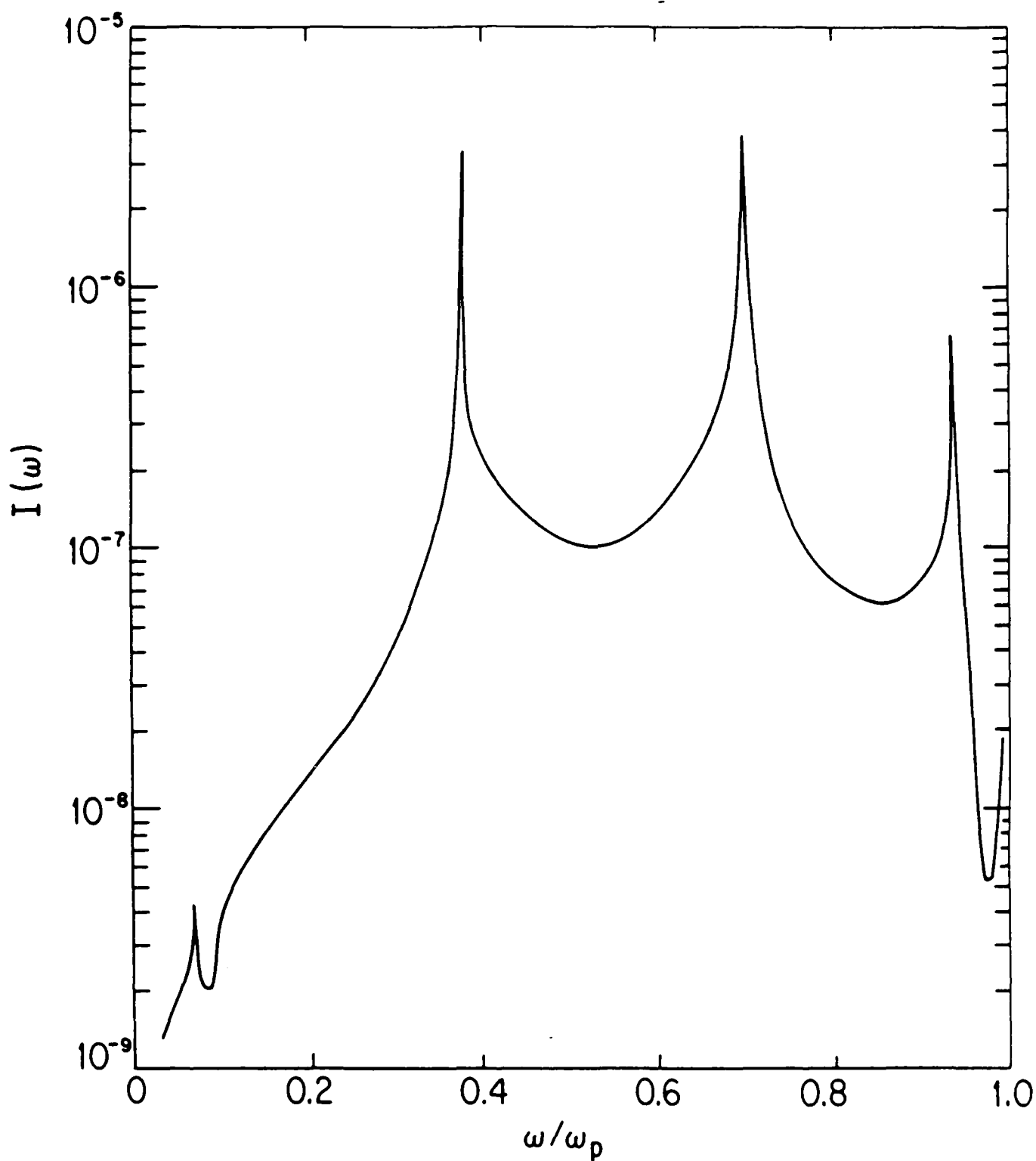
6. Comparison of the exact values of the resonance frequencies and the approximate values given by the analytical expression (20) [solid line] for  $d/a = 0.104$ ,  $h/a = 0.223$  and  $a/R = 0.895$ .



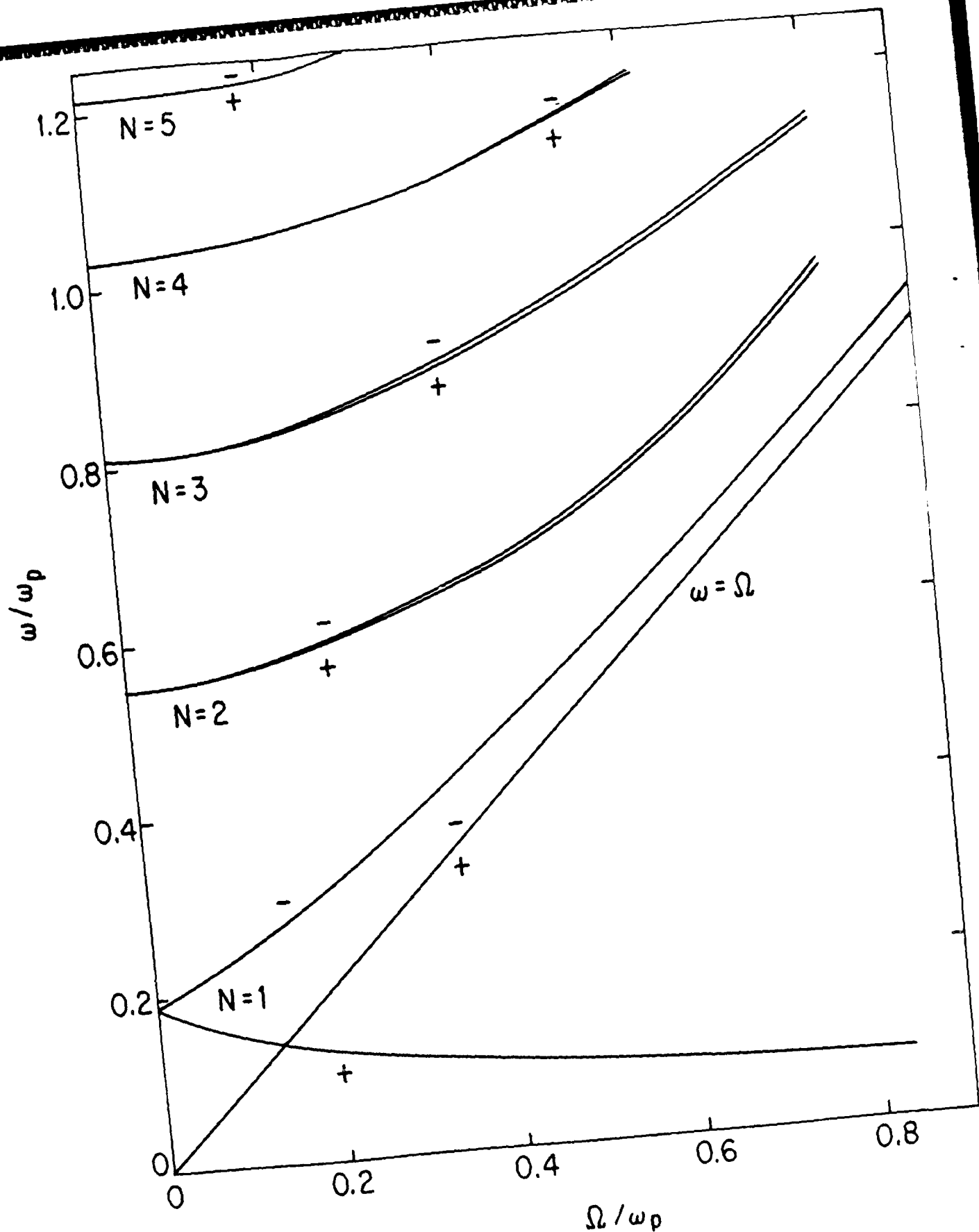
7. Comparison, as a function of  $h/R$ , of exact values of resonance frequencies (circles) and the approximate values given by the analytic expression (20) [solid line] for the  $\ell = 0$ ,  $N = 2$  mode and for  $a/R = 0.895$ ,  $d/h = 0.465$ .



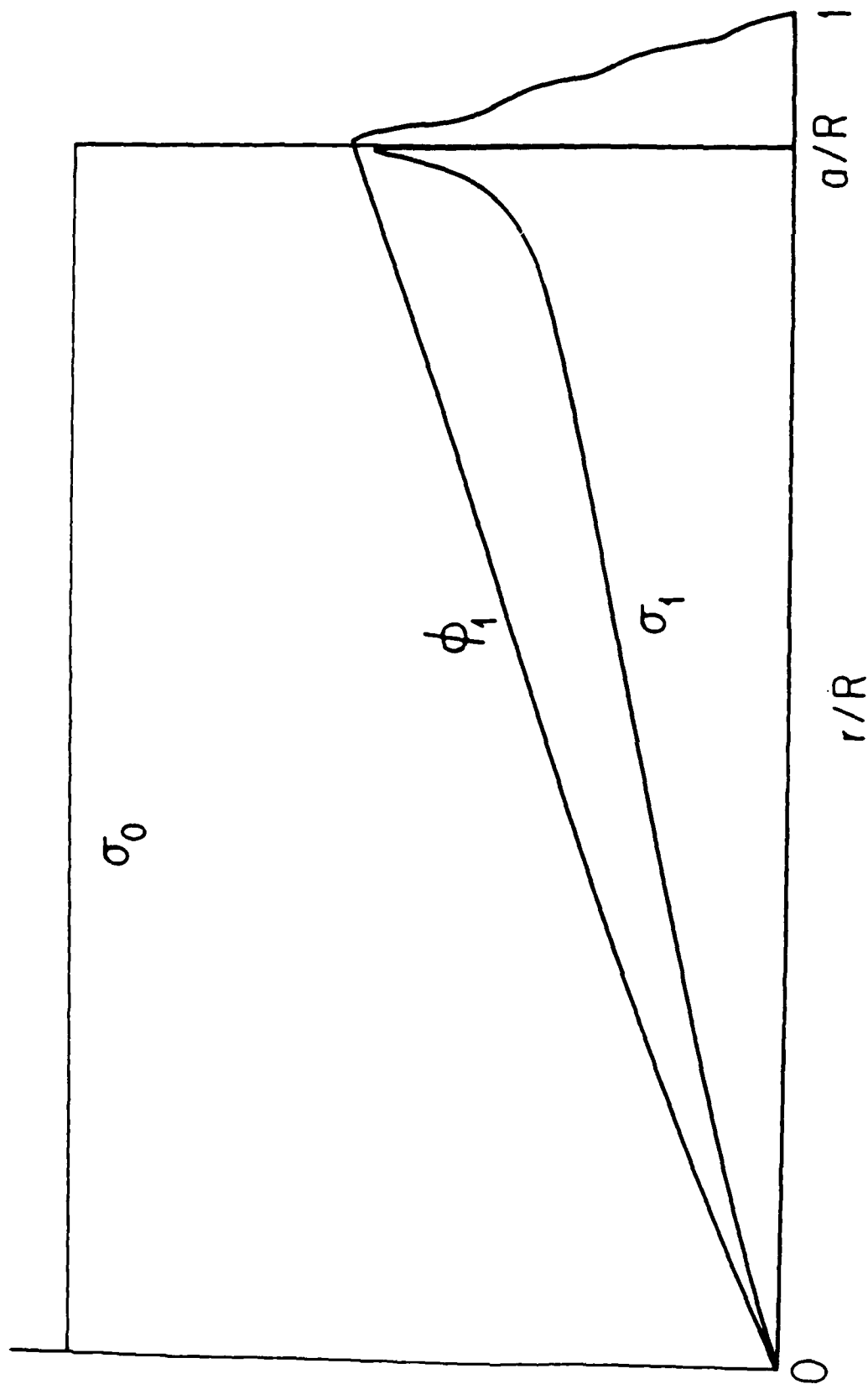
8. Comparison, as a function of  $a/R$ , of exact values of resonance frequencies (circles) and the values given by Eq. (20) [solid line] for the  $l = 0$ ,  $N = 2$  mode and for  $d/R = 0.093$ ,  $h/R = 0.2$ .



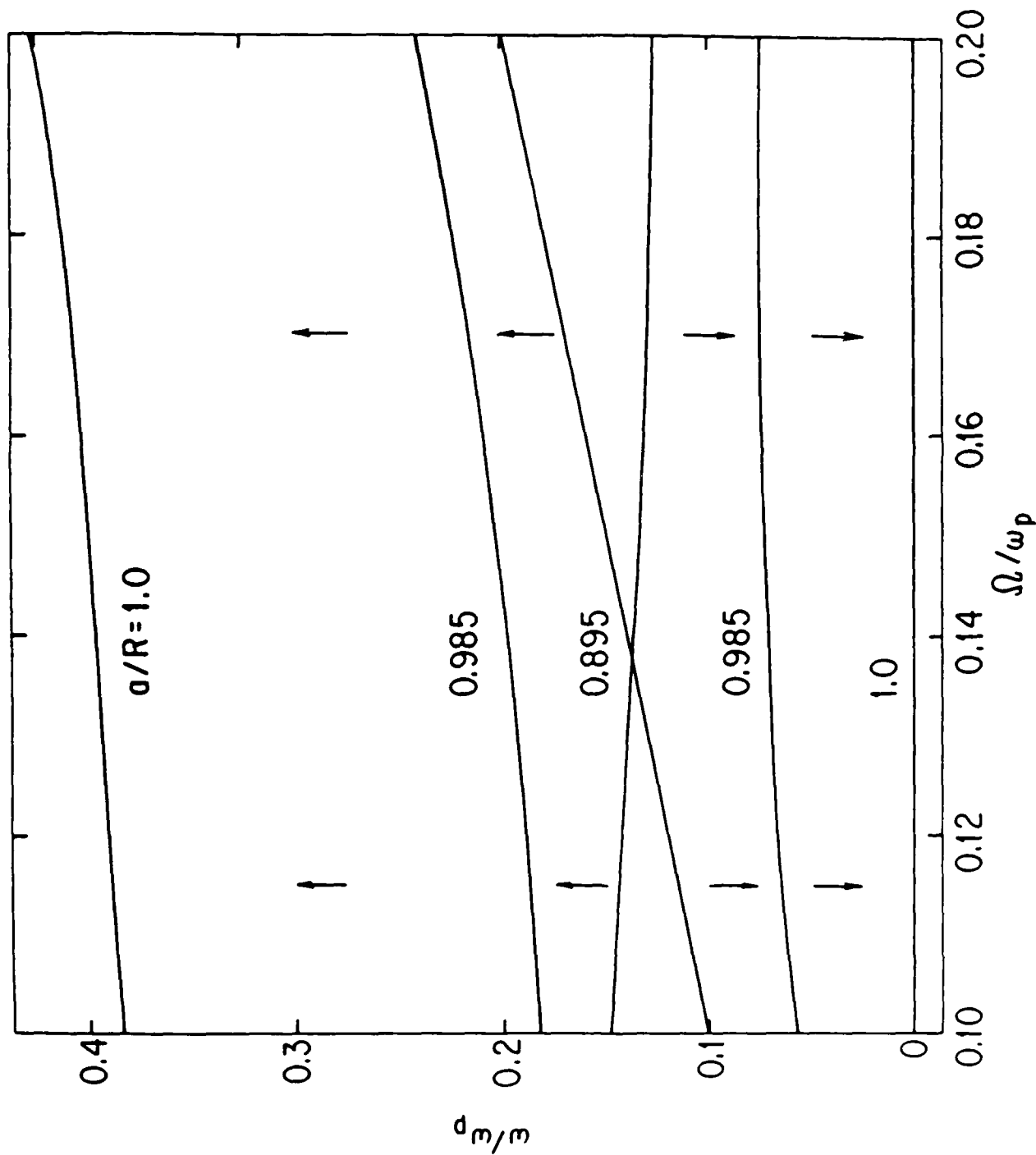
9. Current  $I$  (in amperes) through the center button in the top electrode as a function of the external frequency  $\omega$  [Eq. 28]. The collision frequency  $\nu$  is  $4 \times 10^{-3} \omega_p$  and the driver voltage  $\phi_w = 10\text{mV}$ .



10. Plasma resonances vs.  $\Omega = qB/mc$  for  $\ell = \pm 1$  and for  $d/r = 0.093$ ,  $h/R = 0.2$ ,  $a/R = 0.895$ . The branches designated + (or -) propagate circularly right-handed (or left-handed) with respect to the magnetic field.

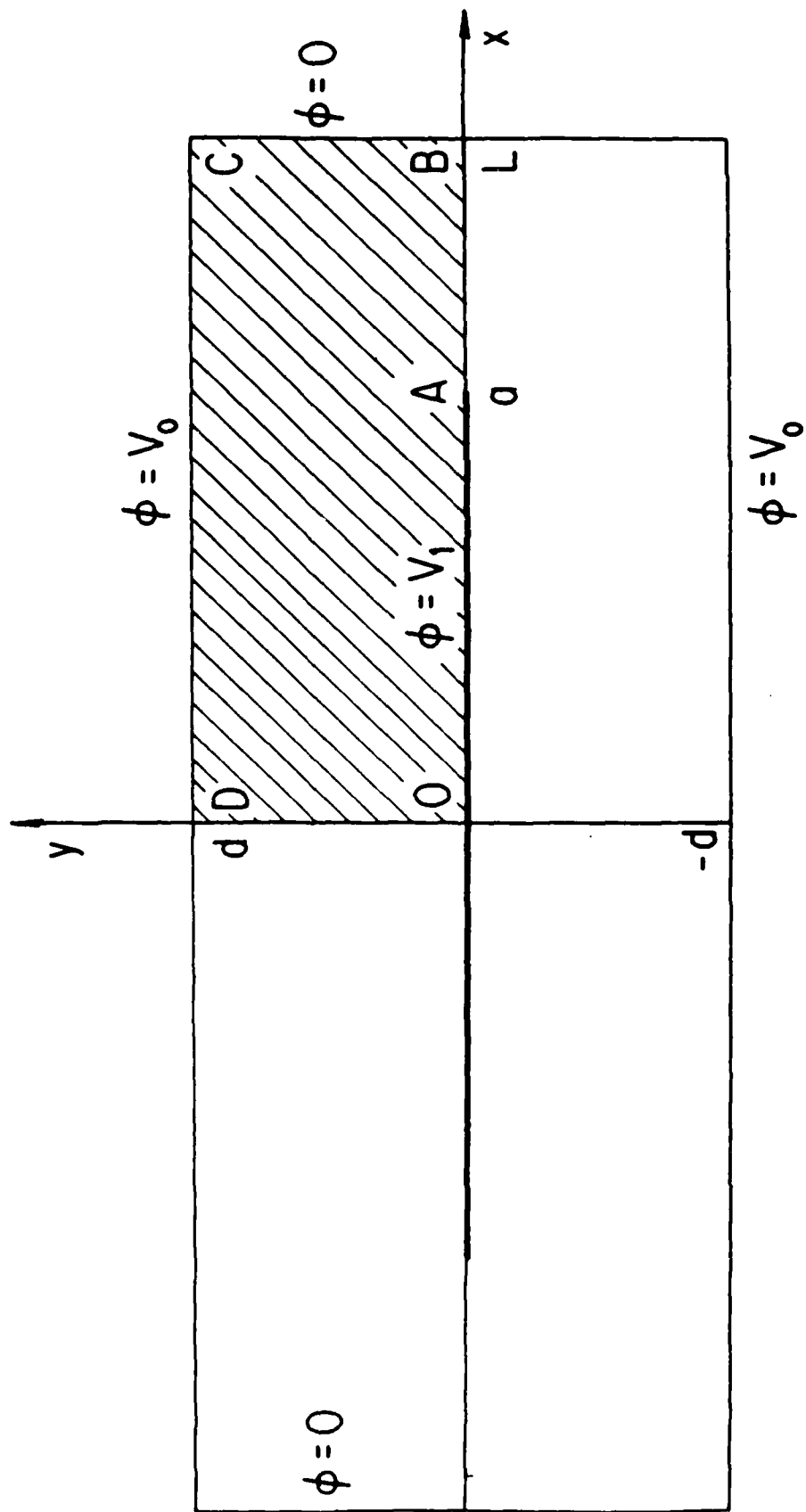


11. Radial dependence of the potential  $\phi_1(r, z=d)$  and density  $\sigma_1(r)$  for the  $\ell = +1$  mode near  $\omega = \Omega$  for  $\Omega/\omega_p = 0.5$ ,  $d/R = 0.093$ ,  $h/R = 0.2$ ,  $a/R = 0.895$ .

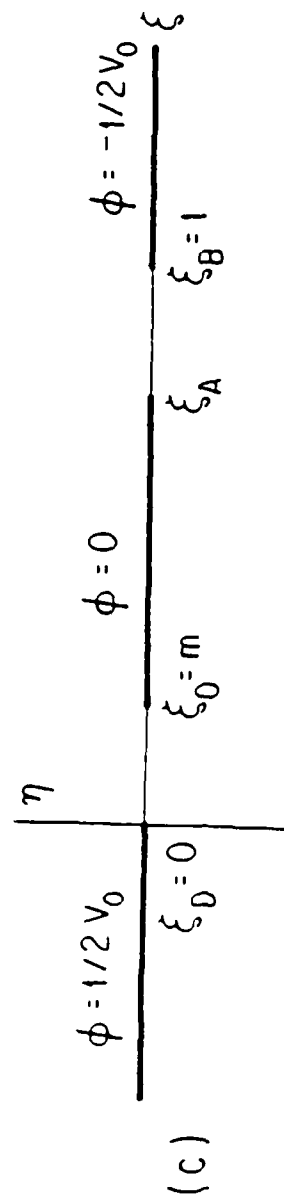
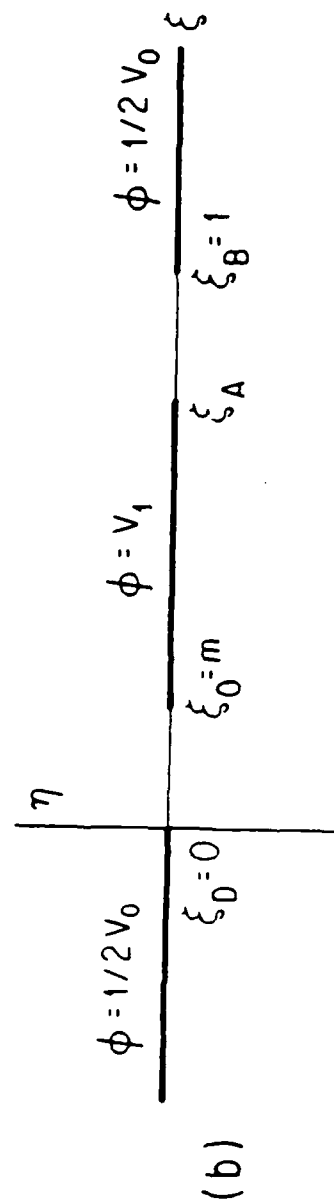
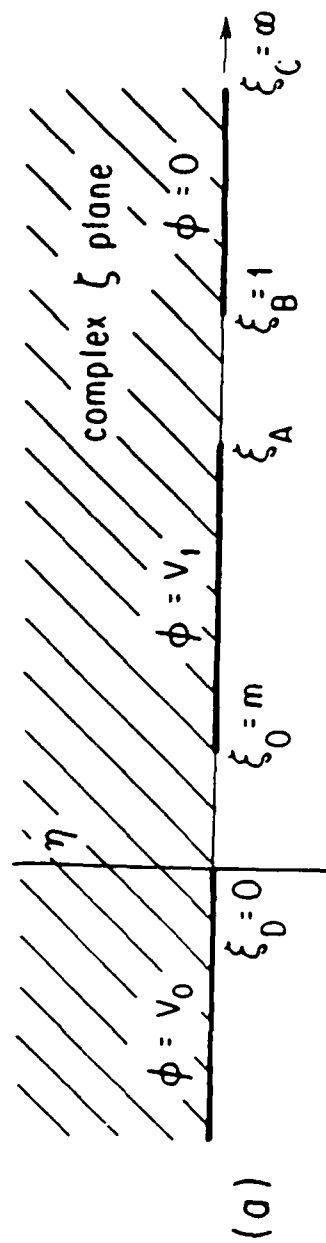


12. An enlargement of the region where the  $\ell = +1$  modes cross in Fig. 10.

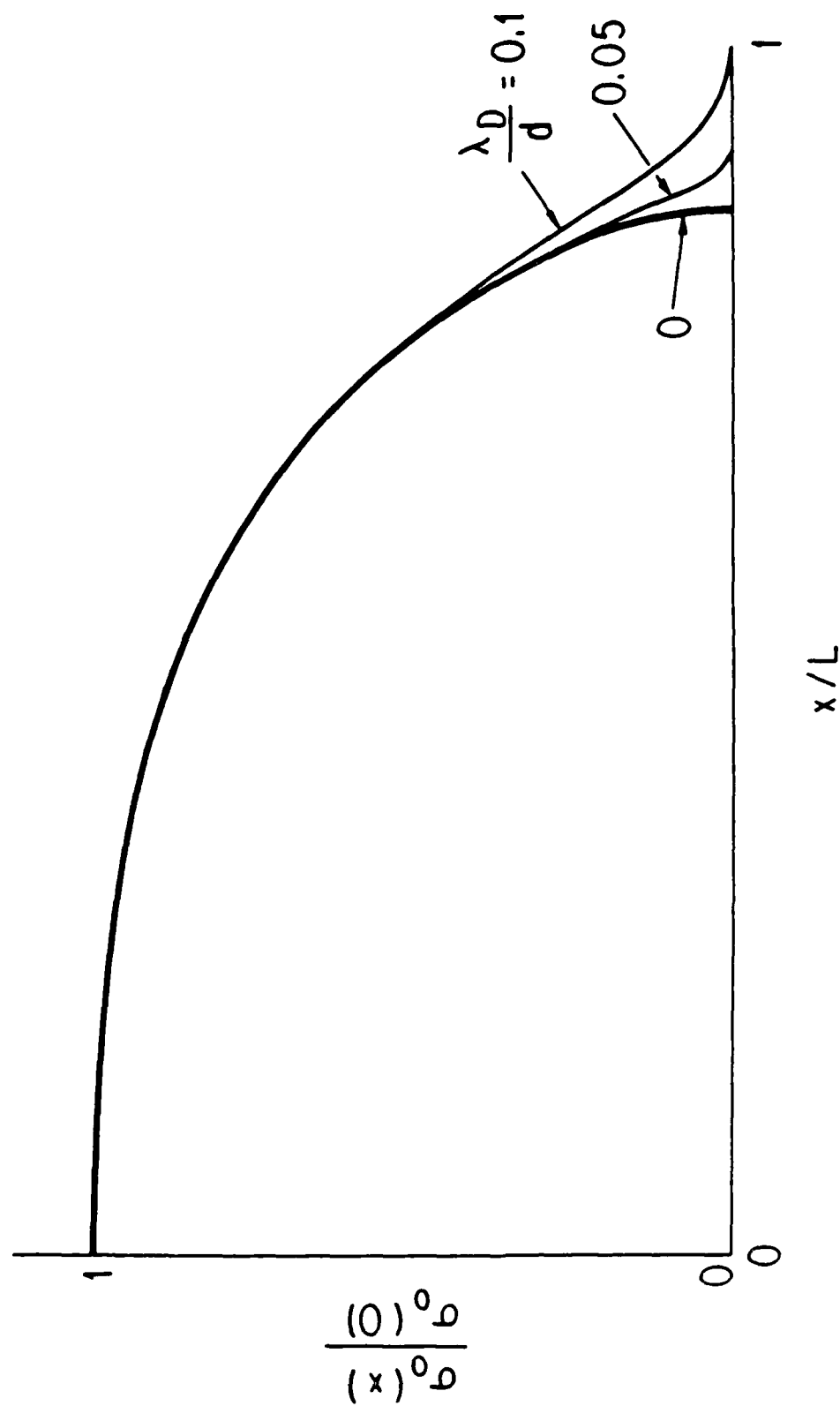
The positions of the branches as  $a/R$  assumes the values 0.895, 0.985 and 1.0 are shown.



13. Cartesian model geometry for the confined two-dimensional plasma layer.

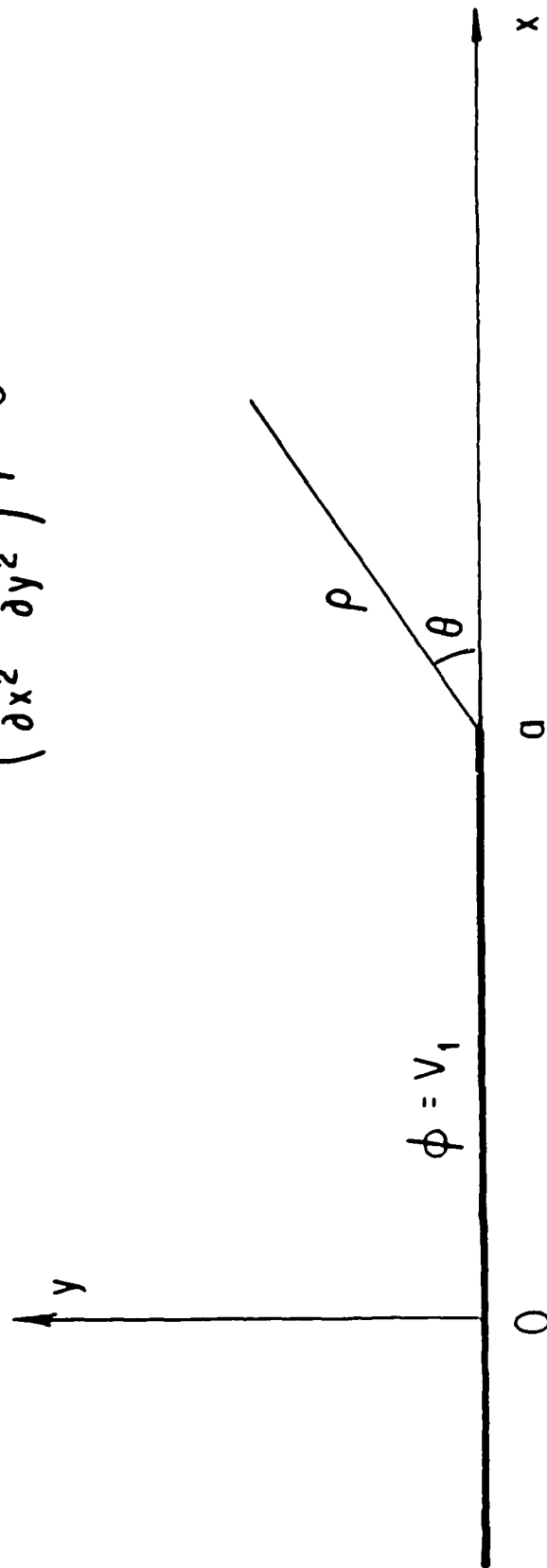


14. a) Complex  $\zeta$ -plane showing the mapping (A1). The shaded area (rectangle OBCD) of Fig. (13) is mapped into the upper half of the  $\zeta$ -plane. The problem can be regarded as a superposition of two potential problems illustrated in (b) and (c).



15. Density profile  $\sigma_0(x)$  given by the analytic expression (A8) for  $d/L = 0.625$  or  $m = 0.1$  (thick line). The other curves are numerical solutions of the Cartesian analogs of Eqs. (1) -(6) for the same geometry, the same  $\sigma_0(0)$  and for  $\lambda_D/d = 0.05$  and  $0.1$ ; the Debye length  $\lambda_D$  is defined as  $\lambda_D = [2dT/4\pi q^2 \epsilon_0(0)]^{1/2}$ .

$$\left( \frac{\partial^2}{\partial x^2} + \frac{\partial^2}{\partial y^2} \right) \phi = 0$$



16. Geometry in the vicinity of the plasma edge  $x = a$ .

- PPG-1048 "Chaotic Behavior and Period Multiplication in Plasmas", P. Cheung, and A.Y. Wong, submitted to Phys. Rev. Lett., March 1987.
- PPG-1049 "Low Activation Ferritic Alloys: Patent Description", D.S. Gelles, N.M. Ghoniem, and R. Powell, March 1987.
- PPG-1050 "The Spectrum, Spatial Distribution and Scaling of Microturbulence in the Text Tokamak", D.L. Brower, W.A. Peebles, and N.C. Luhmann, Jr., submitted to Nucl. Fusion, March 1987.
- PPG-1051 "Predicting the Magnetospheric Plasma of Weather," John M. Dawson, submitted for inclusion in Proc. of the NASA/OAST Workshop on Space Technology Plasma Issues in 2001, 24-26 Sept. 1986, March 1987.
- PPG-1052 "A Kinetic Study of Solar Wind Mass Loading and Cometary Bow Shocks", N. Omid and D. Winske, submitted to JGR, April 1987.
- PPG-1053 "An Analytic Model for Flow Reversal in Diverted Plasmas" P.I.H. Cooke, A.K. Prinja, submitted to Nucl. Fusion Lett., March 1987.
- PPG-1054 "Stability and Tunability of a CARM Amplifier," A. T. Lin and K. R. Chu, April, 1987.
- PPG-1055 "Enhancement of Efficiency and Gain in Cyclotron Autoresonance Masers," T. H. Kho and A. T. Lin, April, 1987.
- PPG-1056 "Observation of a High Density Ion Mode in Tokamak Microturbulence," D. Brower, W. A. Peebles, S. Kim, N. C. Luhmann, Jr., W. M. Tang, and P. E. Phillips, April, 1987.
- PPG-1057 "Simulation of Microscopic Processes in Plasma", Viktor K. Decyk, April, 1987.
- PPG-1058 "A Model of the Plasma Diffusion in Inner Jovian Magnetosphere Incorporating Precipitation-Induced Conductivity" by D. Summers, R.M. Thorne, and Y. Mei, submitted to JGR, April 1987.
- PPG-1059 "Jovian Magnetospheric Diffusion with Variable Loss Rate of Radiation Belt Ions", D. Summers, R.M. Thorne, and Y. Mei, submitted to Planet. Space Sci., April, 1987.
- PPG-1060 "Theory of Centrifugally-Driven Magnetospheric Diffusion", D. Summers, R.M. Thorne and Y. Mei, Astrophys. J., April 1987.
- PPG-1061 "Analytical Solutions for the Growth of Oblique Waves in a Plasma with Field-Aligned Beam", D. Summers and R.M. Thorne, submitted to Phys. Fluids, April 1987.
- PPG-1062 "On the Marginal Stability Criterion for Loss-Cone Distribution" R.M. Thorne and D. Summers, submitted to Proc. Roy. Soc. A, April 1987.
- PPG-1063 "Analytical Solutions for the Growth of Oblique Waves in a Plasma with Ring-Beam", R.M. Thorne and D. Summers, submitted to J. Phys., April 1987.

- PPG-1064 "The Focusing of a Relativistic Electron Beam Using a Preformed Ion Channel", S. Wilks, J.M. Dawson, and T. Katsouleas, submitted to Phys. Rev. A, April 1987.
- PPG-1065 "On MHD Intermediate Shocks," C. C. Wu, to be published to Geophys. Res. Letts., May, 1987.
- PPG-1066 "Development of a Mass - Sensitive Ion Energy Analyzer" G. Hairapetian and R. Stenzel, submitted to R.S.I. May, 1987.
- PPG-1067 "The MHD Intermediate Shock Interaction with an Intermediate Wave: Are Intermediate Shocks Physical?" by C. C. Wu, May, 1987.
- PPG-1068 "Linear Instabilities in Multicomponent Plasmas and their Consequences on the Auroral Zone" D. Schriver and M. Ashour-Abdalla submitted to J.J.R., May, 1987.
- PPG-1069 "Cosmic Ray Acceleration: A Plasma Physicist's Perspective" C.F. Kennel, submitted to Inter. "Rosenbluth Symposium", on Dynamics of Particles and Plasmas, Austin, Texas, February 5-6, 1987.
- PPG-1070 "Ray Tracing Analysis of LH Fast Waves in CCT", T.K. Mau, K.F. Lai, R.J. Taylor, submitted to the 7th APS Conference, Kissimmee Florida, May 4-6 1987.
- PPG-1071 "Combined Wiggler and Solenoidal Field Effects In Free Electron Laser and Electron Cyclotron Maser," T. H. Kho and A. T. Lin, invited paper presented by A. T. Lin at the Fourth International Symposium on Gyrotron and Free Electron Laser, Chegdu, People's Republic of China, May, 1987.
- PPG-1072 "MHD Flow in a Curved Pipe," F. Issicci, N.G. Ghoniem, and I. Catton, submitted to Phys. Fluids, June 1987.
- PPG-1073 "The New Roles of Cavitones in Inhomogeneous Plasmas Under Strong Electromagnetic Irradiation" T. Tanikawa, Ph.D Dissertation.
- PPG-1074 "Progress Report on Pisces: Plasma-Surface Interactions and Materials Research" Pisces Group \*R. W. Conn, D. M. Gobel, Y. Hirooka, B. LaBombard W. K. Leung and R. Nygren. June, 1987.
- PPG-1075 "Self-Consistent Modification of a Fast Tail Distribution by Resonant Fields in Nonuniform Plasmas," G. J. Morales, M. M. Shoucri and J. E. Maggs, submitted to Phys. of Fluids, June, 1987.
- PPG-1076 "Theory and Simulations on Beat Wave Excitation of Relativistic Plasma Waves," W. B. Mori, Ph.D. dissertation, June 1987.
- PPG-1077 "Equilibrium and Wave Properties of Two-Dimensional Ion Plasmas", G.J. Morales and S.A. Prasad, submitted to Phys. of Fluids, June, 1987

END

9-87

DTIC